RESEARCH ARTICLE

Effects of the tropospheric large-scale circulation on European winter temperatures during the period of amplified Arctic warming

Timo Vihma[1] 🔘 | Rune Graversen[2] | Linling Chen[3] 🔘 | Dörthe Handorf[4] |
Natasa Skific[5] | Jennifer A. Francis[6] | Nicholas Tyrrell[1] | Richard Hall[7] 🔘 |
Edward Hanna[7] 🔘 | Petteri Uotila[8] | Klaus Dethloff[4] | Alexey Y. Karpechko[1] |
Halldor Björnsson[9] | James E. Overland[10] 🔘

[1]Finnish Meteorological Institute, Helsinki, Finland

[2]Department of Physics and Technology, University of Tromsø, Tromsø, Norway

[3]Nansen Environmental and Remote Sensing Centre, Bergen, Norway

[4]Alfred Wegener Institute, Helmholtz Center for Polar and Marine Research, Potsdam, Germany

[5]Department of Marine and Coastal Sciences, Rutgers University, New Brunswick, New Jersey

[6]Woods Hole Research Center, Falmouth, Massachusetts

[7]School of Geography and Lincoln Centre for Water and Planetary Health, University of Lincoln, Oakland, California

[8]Atmospheric and Earth System Research (INAR)/ Physics, University of Helsinki, Helsinki, Finland

[9]Icelandic Meteorological Office, Reykjavik, Iceland

[10]NOAA/Pacific Marine Environmental Laboratory, Seattle, Washington

Correspondence
Timo Vihma, Finnish Meteorological Institute, P.O. Box 503, Erik Palmenin aukio 1, 00101 Helsinki, Finland.
Email: timo.vihma@fmi.fi

Abstract

We investigate factors influencing European winter (DJFM) air temperatures for the period 1979–2015 with the focus on changes during the recent period of rapid Arctic warming (1998–2015). We employ meteorological reanalyses analysed with a combination of correlation analysis, two pattern clustering techniques, and back-trajectory airmass identification. In all five selected European regions, severe cold winter events lasting at least 4 days are significantly correlated with warm Arctic episodes. Relationships during opposite conditions of warm Europe/cold Arctic are also significant. Correlations have become consistently stronger since 1998. Large-scale pattern analysis reveals that cold spells are associated with the negative phase of the North Atlantic Oscillation (NAO-) and the positive phase of the Scandinavian (SCA+) pattern, which in turn are correlated with the divergence of dry-static energy transport. Warm European extremes are associated with opposite phases of these patterns and the convergence of latent heat transport. Airmass trajectory analysis is consistent with these findings, as airmasses associated with extreme cold events typically originate over continents, while warm events tend to occur with prevailing maritime airmasses. Despite Arctic-wide warming, significant cooling

has occurred in northeastern Europe owing to a decrease in adiabatic subsidence heating in airmasses arriving from the southeast, along with increased occurrence of circulation patterns favouring low temperature advection. These dynamic effects dominated over the increased mean temperature of most circulation patterns. Lagged correlation analysis reveals that SCA- and NAO+ are typically preceded by cold Arctic anomalies during the previous 2–3 months, which may aid seasonal forecasting.

KEYWORDS

Arctic, European weather, North Atlantic oscillation, Scandinavian pattern, subsidence heating, teleconnections

1 | INTRODUCTION

Coincident with rapid warming in the Arctic, extreme weather events have become increasingly common in mid-latitudes (IPCC, 2012; Munich Re, 2018), with possible causal linkages between these trends (Cohen *et al.*, 2014, 2017; Coumou *et al.*, 2014; Masato *et al.*, 2014; Kug *et al.*, 2015; Overland *et al.*, 2016; Francis, 2017; Vihma, 2017; Vavrus, 2018). Arctic amplification (AA) has been suggested as contributing to an increased occurrence of persistent weather patterns (Petoukhov *et al.*, 2013; Masato *et al.*, 2014; Hanna *et al.*, 2016; Kornhuber *et al.*, 2017; Mann *et al.*, 2017; Francis *et al.*, 2018), and especially to winter cold spells in mid-latitudes, mainly in East Asia (Kug *et al.*, 2015) and North America (Francis, 2017; Cohen *et al.*, 2018; Overland and Wang, 2018) but also in the United Kingdom (Hanna *et al.*, 2017). However, potential Arctic effects on continental Europe in winter have remained less clear (Overland *et al.*, 2015), owing to other forcings from different locations, for example, from the North Atlantic and tropics (Cassou *et al.*, 2004; Buckley and Marshall, 2016; Zappa and Shepherd, 2017), which makes it challenging to distinguish the impacts from the Arctic.

It is known that the negative phase of the North Atlantic Oscillation (NAO) is associated with anomalously cold and dry winters in most of Europe, whereas the positive phase of NAO is often associated with anomalously warm and moist winters (Marshall *et al.*, 2001a; Hurrell *et al.*, 2003; Hanna and Cropper, 2017). However, the NAO phase alone does not explain all aspects of the influence of atmospheric circulation over the North Atlantic on Europe (Vautard, 1990). The state of atmospheric circulation in the North Atlantic region also varies with episodes of Greenland Blocking (Hanna *et al.*, 2016, 2018), the Scandinavian Pattern (Bueh and Nakamura, 2007), East-Atlantic Pattern (Barnston and Livezey, 1987; Bojariu and Reverdin, 2002), and the East Atlantic/West Russia Pattern (Lim, 2015) that also influence European winter weather. Furthermore, Arctic and North

Atlantic influences on Europe are connected. In addition to linkages through Greenland Blocking, evidence for connections is apparent in the following: (a) synoptic and large-scale circulation over the North Atlantic and Nordic seas strongly affects the occurrence and strength of Arctic cold-air outbreaks and polar lows reaching Europe (Kolstad *et al.*, 2009), and (b) several recent studies suggest that amplified Arctic warming favours a negative NAO (Kim *et al.*, 2014; Vihma, 2014; Francis and Skific, 2015; Nakamura *et al.*, 2015; Deser *et al.*, 2016), albeit not consistently (Singarayer *et al.*, 2006; Screen *et al.*, 2014; Smith *et al.*, 2017).

During 1956 to 2005, cold winters in Europe seem rarely linked with negative sea-ice anomalies in the Arctic (Yang and Christensen, 2012), but in recent years of dramatically reduced sea ice, there are indications that this relationship has appeared and is becoming increasingly robust. Grassi *et al.* (2013) notes that Barents–Kara sea-ice reduction favours a wintertime increase in the occurrence and intensity of extreme cold events over continental Europe along with extreme precipitation events over the Mediterranean basin. Observed reductions in autumn–winter Arctic sea ice, especially in the Barents and Kara seas, are correlated with strengthened anticyclonic circulation anomalies over the Arctic Ocean, which tend to induce easterly flow and cold-air advection over northern Europe (Cohen *et al.*, 2014). Model simulations suggest that sea-ice decline in the Canadian Archipelago and Baffin-Bay links with cold-air outbreaks over central Europe during October–March (Screen, 2017). In these months, sea-ice loss in the Barents–Kara Seas results in drying over northwest Europe and a decrease in 500 hPa geopotential heights extending from the mid-Atlantic to eastern Europe at roughly 40°N, resembling a negative phase of the NAO. According to Koenigk *et al.* (2016), winter temperatures in central and western Europe are most strongly correlated with Greenland sea-ice variability.

The most direct effect of AA on mid-latitude winter weather is that cold-air outbreaks originating from the Arctic

are not as cold as they were in the 1980s and 1990s (Serreze *et al.*, 2011; Screen, 2014), except in East Asia (Kim *et al.*, 2014). However, the Arctic's influence is often transmitted via more complex mechanisms, including changes in (a) latitude, speed, and meandering of the polar front jet stream (Vavrus *et al.*, 2017; Zappa *et al.*, 2018), (b) blocking occurrence, strength, and location (Masato *et al.*, 2014; Hanna *et al.*, 2016, 2018), and (c) wintertime stratosphere–troposphere coupling (Handorf *et al.*, 2015; Kretschmer *et al.*, 2016; Crasemann *et al.*, 2017; Hoshi *et al.*, 2019).

This study addresses the question: How does the tropospheric large-scale circulation affect European air temperatures in winter (defined as DJFM), and have these effects changed during the period of AA? We address years 1979–2015, focusing on differences between the first and second half of the period, the latter corresponding to the start of the rapid AA (Vavrus *et al.*, 2017; Davy *et al.*, 2018; Overland *et al.*, 2019). The study is based on atmospheric reanalysis products that are analysed by applying a range of methods. Using multiple approaches allows us to address the occurrence of daily air temperature extremes in Europe and the Arctic, large-scale circulation patterns affecting European weather, and origin of air masses advected to Europe.

2 | METHODS

2.1 | Analyses of air temperature anomalies

Five study regions of Europe were chosen: CE: Central Europe 45°–55°N, 0°–20°E; SE: Southern Europe 35°–45°N, 10°W–35°E; NE: Northern Europe 55°–70°N, 5°–25°E; WE: Western Europe 50°–60°N, 10°W–5°E; EE: Eastern Europe 45°–55°N, 20°–40°E (Figure 1). Data for 2-m air temperatures (T2m) were obtained from the ERA-Interim reanalysis (Dee *et al.*, 2011) for 1979 to 2015. For each region the mean area-weighted T2m for the region was calculated for each day, and then converted to standardized anomalies relative to 1981–2010 climatology for each day, removing the seasonal cycle. Extreme temperature anomaly events in each region were defined as the detrended temperature anomaly being greater than or equal to +1.75 standard deviation (SD) for at least four consecutive days for the positive anomalies (hereafter called as warm events), and less than or equal to −2 SD for at least four consecutive days for the negative anomalies (hereafter called as cold events). The different thresholds for positive and negative anomalies were applied to ensure samples of similar size.

Trends in the number of days when warm/cold events occurred were assessed for significance (95% confidence) using the Mann–Kendall trend test, with consideration of

autocorrelation in the time series (Yue and Wang, 2004). In order to demonstrate the possible relation of these events with AA, we created composite maps of Northern Hemisphere T2m related to the cold/warm events in these five regions.

Central Arctic warm events are defined as periods of four or more consecutive days when the detrended T2m anomaly, averaged over 70–90°N, is greater than 1.75 SD above the 1981–2010 climatology. Greenland blocking episodes are identified as four or more consecutive days when the Greenland Blocking Index (GBI) is more than 2 SD above 1981–2010 climatology (Hanna *et al.*, 2018). The GBI is defined using the mean 500 hPa geopotential height for the 60–80°N, 20°–80°W region (Hanna *et al.*, 2016).

2.2 | Analyses of large-scale circulation

Self-organizing maps (SOM; Kohonen, 2001) were applied to classify daily ERA-Interim 500 hPa geopotential height anomaly fields throughout 1979–2015 in the region 30°–80°N, 60°W–60°E. The SOM algorithm is initialized using the first two EOFs of the data vectors to ultimately create a matrix of representative spatial patterns, with the matrix size defined by the user. In the SOM training, individual geopotential height anomaly fields are presented to the SOM and a Euclidean measure of distance is compared between the anomaly field and each pattern to determine the "winning" pattern, which has the smallest Euclidean distance to the anomaly field. As each new field is presented, the
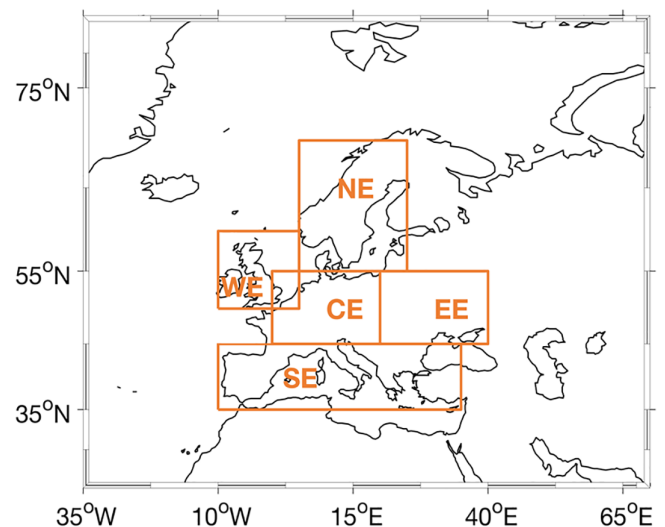

FIGURE 1 Map of five European areas. CE: Central Europe 45°–55°N, 0°–20°E; SE: Southern Europe 35°–45°N, 10°W–35°E; NE: Northern Europe 55°–70°N, 5°–25°E; WE: Western Europe 50°–60°N, 10°W–5°E; EE: Eastern Europe 45°–55°N, 20°–40°E [Colour figure can be viewed at wileyonlinelibrary.com]

winning pattern and neighbouring patterns are updated iteratively reducing the difference against the anomaly field (Hewitson and Crane, 2002). In this way the SOM algorithm organizes the patterns (also called nodes) so that similar daily fields are clustered into one pattern, and the patterns are presented such that those most different from each other are in the opposite corners of a two-dimensional array of "self-organized" patterns as shown in Figure 2. The SOM algorithm objectively classifies atmospheric circulation anomalies; this approach objectively identifies weather patterns that affect European temperatures.

We selected a matrix size of 12 as a suitable number of nodes as a balance between identifying distinct patterns and providing sufficient detail. We then identified the most frequently occurring patterns and named them according to the well-known large-scale circulation patterns that they resemble. The SOM algorithm keeps track of which daily fields belong in each of the 12 patterns. This allowed us to project other variables of interest (such as anomalies of T2m and divergence of the dry-static energy and latent heat) onto the 12 circulation patterns. We also calculated the frequency of occurrence of each pattern, as well as frequency changes from 1979–1997 to 1998–2015.

The vertically integrated latent heat transport in the zonal and meridional directions is given by:

$$uE_Q = \int_0^{P_s} u\,L\,q\,\frac{dp}{g} \tag{1}$$

and

$$vE_Q = \int_0^{P_s} v\,L\,q\,\frac{dp}{g}, \tag{2}$$

where E_Q is the latent heat, u and v are zonal and meridional wind components, L is specific heat of condensation, q is air specific humidity, g is acceleration due to gravity, and p is pressure (subscript s referring to Earth surface). Transports were computed using variables at all ERA–Interim model hybrid levels, a 6-hr time resolution, and interpolated to 0.5 × 0.5° horizontal grid. Due to a mass-flux inconsistency in reanalysis data (Trenberth, 1991), a barotropic mass-flux correction was applied to the wind field at each time step before the energy transport was calculated (Graversen, 2006). After computing the transports, the divergence of the vertically integrated transport and its anomaly was calculated. Analogous calculations yielded the anomaly of the divergence of vertically integrated transport of dry-static energy (in the equations, $L\,q$ was replaced by $c_p T + g\,z$, where c_p is the specific heat capacity at constant pressure, T is air temperature, and z is height). Spatial correlation
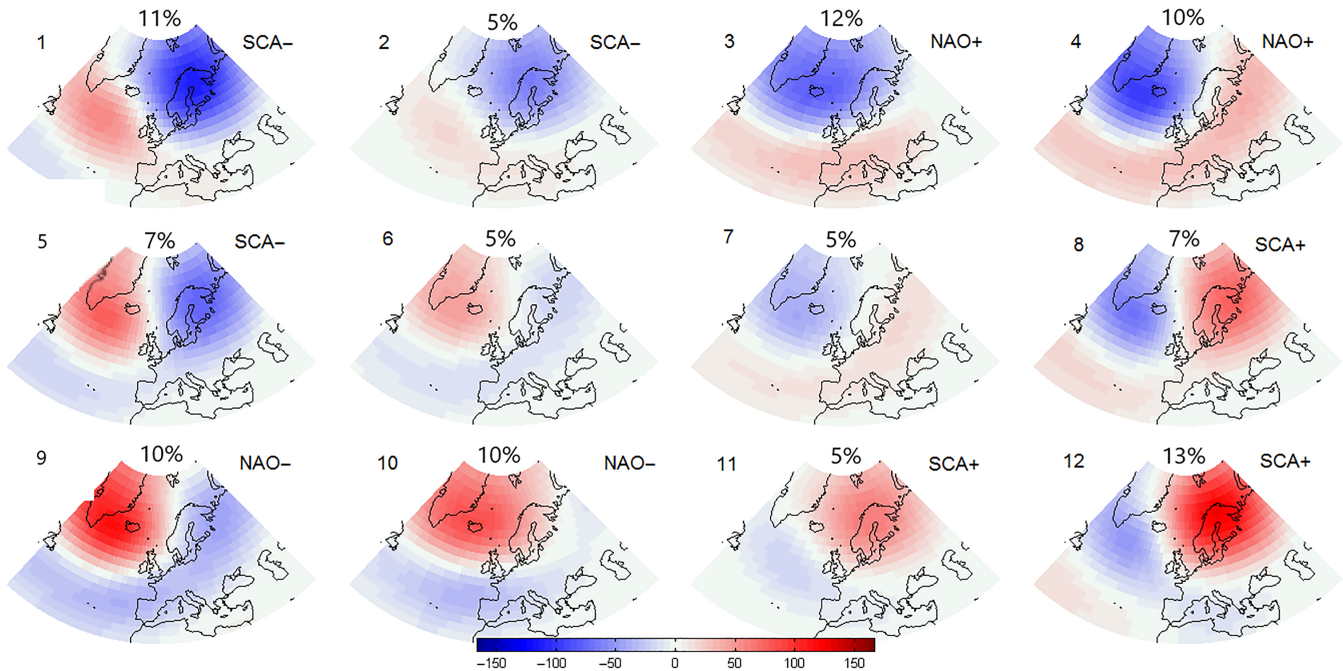

FIGURE 2 Self-organizing maps (SOMs) generated using 500 hPa height anomalies from ERA-interim reanalysis, 1979–2015. The patterns are numbered from 1 to 12, and most are named after the large-scale circulation patterns they resemble. The percentages above each pattern denote their relative frequency of occurrence

coefficients were calculated to quantify the relationship between the time-averaged fields of transport divergences and T2m anomalies.

To understand how the large-scale circulation patterns—as represented by the SOM nodes—that affect European weather are associated with Arctic temperatures, the T2m anomalies averaged over the circumpolar Arctic north of 70°N were calculated 90 days before and after the occurrence of the six most common SOM nodes (nodes 1, 3, 4, 9, 10, and 12).

As the results may be sensitive to the analysis methods and metrics, we also applied a different cluster analysis method (k-means cluster) to the same ERA-Interim fields to identify the most common 500 hPa circulation patterns over Europe and their changes. The cluster analysis was carried out over the North-Atlantic–Eurasian region (30°–90°N, 90°W–90°E) for winter. We have chosen this region due to the increased evidence for dynamical pathways linking Arctic sea-ice anomalies over the Barents–Kara seas to cold Eurasian temperatures in mid-to-late winter.

The daily 500 hPa geopotential height anomaly fields from ERA-Interim for the period 1979–2014 were analysed. We applied the same methodology as in Crasemann et al. (2017), which involves the reduction of the dimensionality of the data set by an Empirical Orthogonal Function (EOF) analysis and a subsequent k-means cluster analysis in the reduced state space spanned by the first five EOFs. As with SOM and other cluster algorithms, it is necessary to prescribe the number of clusters k as an input parameter. Here, we realize the identification of the most common 500 hPa circulation patterns by searching for non-Gaussian structures in the reduced state space (Cassou et al., 2004; Dawson and Palmer, 2015). By performing Monte-Carlo simulations, we tested the null hypothesis of the non-existence of non-Gaussian structures, that is, multi-normal distribution of the probability density function, with the same approach as in Straus et al. (2007), and Dawson and Palmer (2015). Significance of the clustering has been estimated for k = 2–8 … clusters. k = 5 is the smallest significant partition size which is significant at the 95% level, therefore it is used as cluster size. By calculating histograms separately for periods 1979–1997 and 1998–2015, we detected changes in the relative frequency of occurrence of each circulation pattern in each of the winter months. The significance of the changes in each month was tested using a bootstrap test with 1,000 bootstrap replicates for each regime and each month.

2.3 | Analyses of airmass origin

To address the relationship of temperature anomalies with airmass transport into Europe, 5-day backward trajectories were calculated for each day in 1979–2015 ending over 10 selected European cities: Archangelsk, Berlin, Bucharest, Glasgow, Hammerfest, Helsinki, Kazan, Minsk, Moscow, and Rome. These cities were selected with an emphasis on northeastern Europe. The trajectories were calculated by applying the Meteorological Data Explorer (METEX) calculation service (Zeng et al., 2010), which utilizes the NCEP-CFSR reanalysis (Saha et al., 2010) with a spatial resolution of 0.5 × 0.5°. The METEX output includes hourly values along the trajectory of latitude, longitude, horizontal and vertical wind components, air temperature, atmospheric pressure, and the height above ground level. Accordingly, for each city and each day, we determined whether the trajectory start point (airmass origin) was in the Arctic (north of 70°N) and if it was located to the northeast, southeast, southwest, or northwest of the city in question. To avoid trajectories within the atmospheric boundary layer, where reanalyses are more prone to errors, the trajectories were set to end at the height of 1,000 m above each city in question. Information on the air temperature and atmospheric pressure at the trajectory start and end points allowed estimation of the adiabatic subsidence heating (SH), assuming that the potential temperature remains constant during the 5-day airflow along the trajectory:

$$SH = T_S \left(\frac{P_E}{P_S}\right)^{R/c_p} - T_S \qquad (3)$$

where T is the air temperature, P is the atmospheric pressure, R is the gas constant of dry air, and c_p is the specific heat. Subscripts S and E refer to the trajectory start and end points, respectively. Daily results of SH were averaged separately for periods 1979–1997 and 1998–2015. Finally, the distributions of airmass origin and related temperature changes between 1979–1997 and 1998–2015 were analysed utilizing results of the large-scale circulation patterns identified by the cluster analyses.

3 | RESULTS

3.1 | Air temperature anomalies over Europe and the Arctic

Our analyses demonstrate that cold winter events, at least 4 days long, in all five European regions are significantly related to positive temperature anomalies in the Arctic. In WE, CE, and NE, cold winter events are strongly associated with positive T2m anomalies over the Greenland/Baffin region. In SE and EE, however, cold winter events are associated with warm episodes in both the Greenland region and the Barents–Kara seas area (Figure 3, left column). The wintertime association of cold events in Europe and warm events in the central Arctic has become stronger: only two
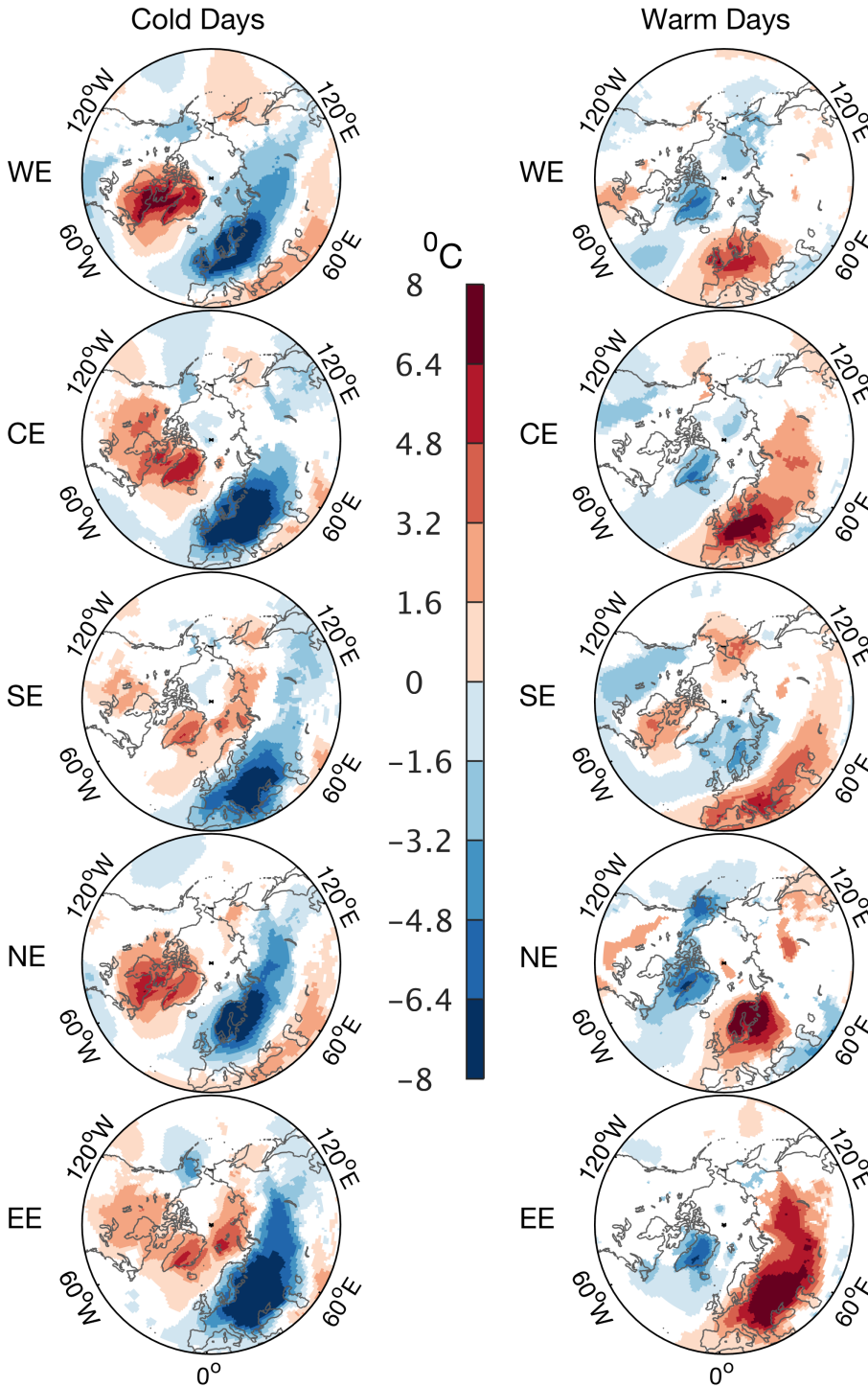
FIGURE 3 Composite maps of the northern hemisphere T2m anomalies related to (1ST column) extremely cold events (−2SD as threshold) and (second column) extremely warm events (+1.75SD as threshold) in western (WE), central (CE), southern (SE), northern (NE), and eastern Europe (EE) during winters (DJFM) 1979–2015. The colour shadings denote the areas with significant (95% confidence) differences between the mean values of composites of anomalous events and the normal events (less than +1.75SD and greater than −2SD). The colour shadings denote the areas with significant (95% confidence) differences between the mean values of composites of anomalous events and the normal events (less than +1.75SD and greater than −2SD)

combined occurrences meet the threshold and duration criteria (Section 2.1) during 1979–1997 out of 42 European regional cold events, but 15 joint Arctic warm/European cold events out of 23 regional warm events occur during 1998–2015. Results are qualitatively similar for detrended data (Table 1). The association with Greenland Blocking events has also become stronger (Table 1), which is not due to increase of cold events but due to increase in simultaneous occurrence of GBI events and European cold events.

The opposite is also true. Warm winter events in all five European regions are associated with cold anomalies in the Arctic, but with remarkable regional differences (Figure 3, right column). Warm events in WE, CE, EE, and NE are associated with cold anomalies in Greenland and, in the case of NE, also in Alaska. However, warm events in SE are associated with cold anomalies in NE, the Nordic Seas, and central and northwestern North America, as well as with warm anomalies in the Labrador–Baffin region.

TABLE 1 Number of cold events in each European region that are preceded by (up to 5 days) or synchronous with warm Arctic (+1.75 SD criteria) and positive GBI (+2 SD criteria) events (left), out of the total number of cold events in each region (right)

Region	Trend retained				Detrended			
	Warm Arctic		GBI		Warm Arctic		GBI	
	1979–1997	1998–2015	1979–1997	1998–2015	1979–1997	1998–2015	1979–1997	1998–2015
Western Europe	0/10	1/4	2/10	3/4	1/6	1/7	2/6	4/7
Southern Europe	0/5	4/4	0/5	1/4	0/4	3/5	0/4	1/5
Central Europe	1/8	2/3	0/8	2/3	1/7	0/4	0/7	1/4
Eastern Europe	1/9	6/8	0/9	1/8	0/7	4/8	0/7	2/8
Northern Europe	0/10	2/4	3/10	1/4	1/6	1/11	2/6	3/11
Total	2/42	15/23	5/42	8/23	3/40	9/35	4/40	11/35

Note: In each case, events are four or more continuous days above or below the defined threshold. Note that cold events in European regions can occur simultaneously and may be associated with the same Arctic warm event or Greenland blocking.

As the number of extreme events per winter is very small (often zero), we calculated inter-annual correlations relaxing the 4-day criteria, that is, addressing individual days passing the 1.75 SD or 2 SD criteria. There are significant positive correlations between the number of cold days per winter in Europe and the number of warm days per winter in Greenland and Barents–Kara seas (Table 2). This demonstrates that in terms of inter-annual variability between winters, cold conditions in WE, NE, and CE are associated with warm conditions in the Greenland region, while cold in EE and SE are associated with a warm Barents–Kara seas area. In contrast, all correlations between the number of warm days per winter in the five European regions and the number of cold days per winter in Greenland and Barents–Kara seas area are insignificant and mostly very close to zero (not shown). As a summary, the results demonstrate a simultaneous correspondence between cold anomalies in the Arctic and warm events in the five European regions (Figure 3, right column), but that the Europe–Arctic relationship is weak in terms of inter-annual variations in the number of warm winter days in Europe and cold winter days in the Arctic.

Changes in these relationships over time are observed by comparing correlations between 1979–1997 and 1998–2015

(Table 2). Statistical relationships between the number of cold days in CE and NE and warm days in Greenland have become consistently stronger during the AA era, as have relationships between cold days in SE and EE and warm days in the Barents–Kara seas region.

As a summary, synoptic-scale linkages between the Arctic and Europe are evident, and have become stronger during the AA, but the analyses presented above do not prove causality.

3.2 | Large-scale circulation patterns controlling European weather

3.2.1 | Results based on SOM analyses

The most frequently occurring SOM patterns in descending order are 12, 3, 1, 4, 9, and 10 (Figure 2). Some of the nodes closely resemble patterns that are recognized as important for European weather: the NAO in its positive phase (nodes 3 and 4, hereafter called NAO+ nodes) and negative phase (9 and 10, NAO- nodes, also associated with the Greenland/Baffin-Bay blocking), as well as the Scandinavian Pattern in its positive (8, 11, and 12; SCA+) and negative phase (1, 2, and 5; SCA-, also called as Atlantic ridge).

TABLE 2 Correlation coefficients between the number of extremely warm days per winter (+1.75SD, without 4-day criterion) in the two Arctic areas and the number of extremely cold days per winter (−2SD, without 4-day criterion) in five European areas

Europe region	Greenland/Baffin (warm)			Barents–Kara Sea (warm)		
	P1	P2	P3	P1	P2	P3
WE (cold)	**0.50**	**0.50**	**0.51**	−0.01	0.10	0.26
CE (cold)	**0.36**	0.33	**0.51**	0.31	0.24	0.33
SE (cold)	0.10	0.03	0.16	**0.36**	0.17	**0.78**
NE (cold)	**0.47**	0.38	**0.58**	0.13	0.27	−0.13
EE (cold)	0.17	0.17	0.18	**0.34**	0.34	**0.53**

Note: Numbers in bold denote significant correlation with a 95% confidence. P1 indicates period of 1979–2015; P2 is 1979–1997; and P3 is 1998–2015.
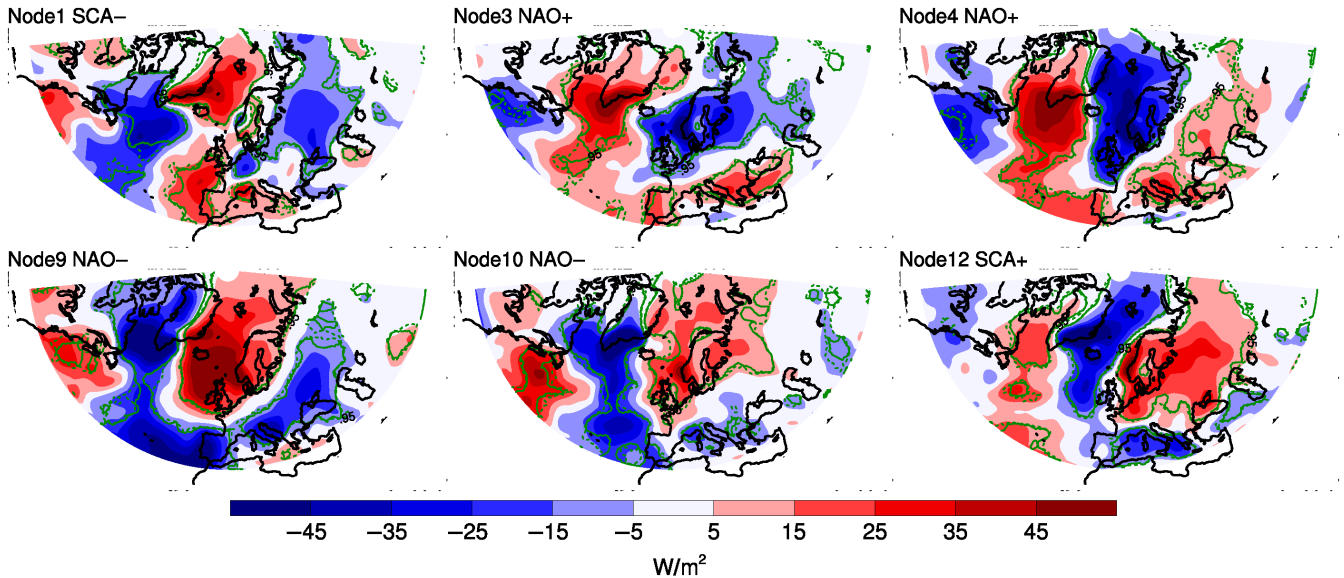
FIGURE 4 Winter (DJFM) anomalies of the divergence of vertically integrated latent heat transport mapped to the six most common nodes of the SOM matrix in Figure 2. Anomalies are relative to monthly climatology of 1979–2015. Dotted and solid green contours enclose areas with significant values at the 95 and 99% level, respectively. The significance is determined using a Monte-Carlo approach, where the anomaly has been compared with 5,000 artificial anomalies that are similar to the original anomaly, but based on a random selection of days from the winter season during the study period

FIGURE 5 Winter (DJFM) anomalies of the divergence of vertically integrated dry-static energy transport mapped to the six most common nodes of the SOM matrix in Figure 2. Anomalies are relative to monthly climatology of 1979–2015. Dotted and solid green contours enclose areas with significant values at the 95 and 99% level, respectively. The significance is determined using a Monte-Carlo approach, where the anomaly has been compared with 5,000 artificial anomalies that are similar to the original anomaly, but based on a random selection of days from the winter season during the study period
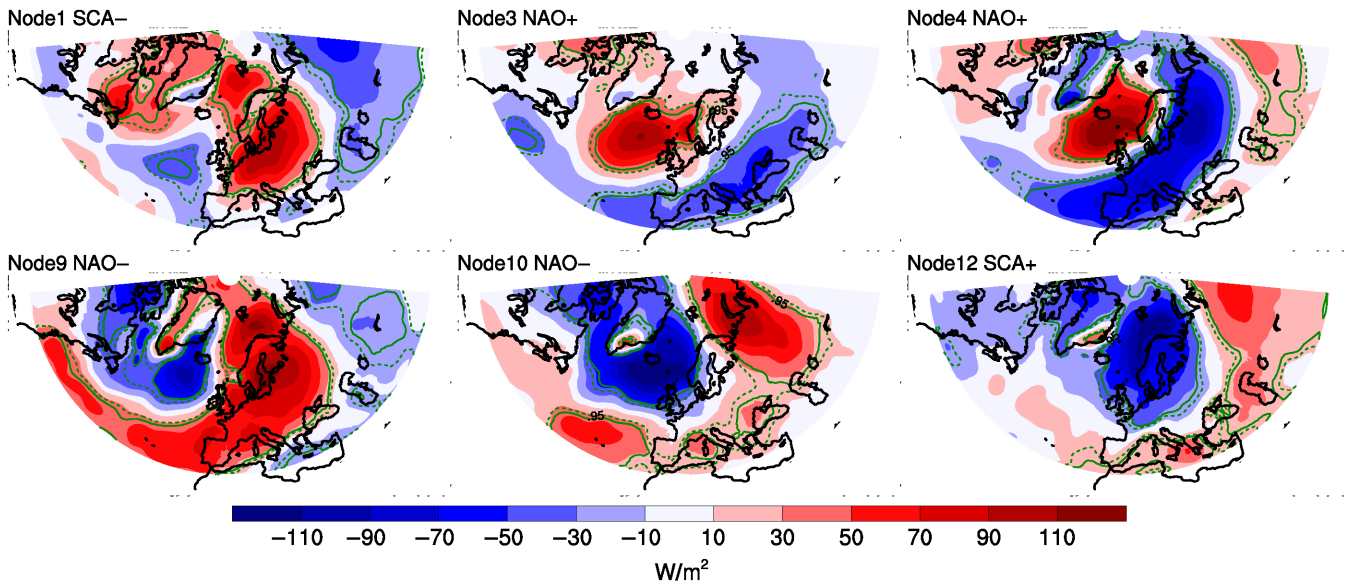
To understand the mechanisms responsible for the association of these circulation patterns with European winter temperatures, we compare the transport divergence anomalies of latent heat (Figure 4) and dry-static energy (Figure 5) projected on the SOM nodes against T2m anomalies (Figure 6).

For clarity, only the six most common nodes are shown in Figures 4–5, and 6.

The results demonstrate that over northern Europe the NAO+ nodes exhibit anomalous convergence of latent heat transport (i.e., negative anomaly in divergence, favouring
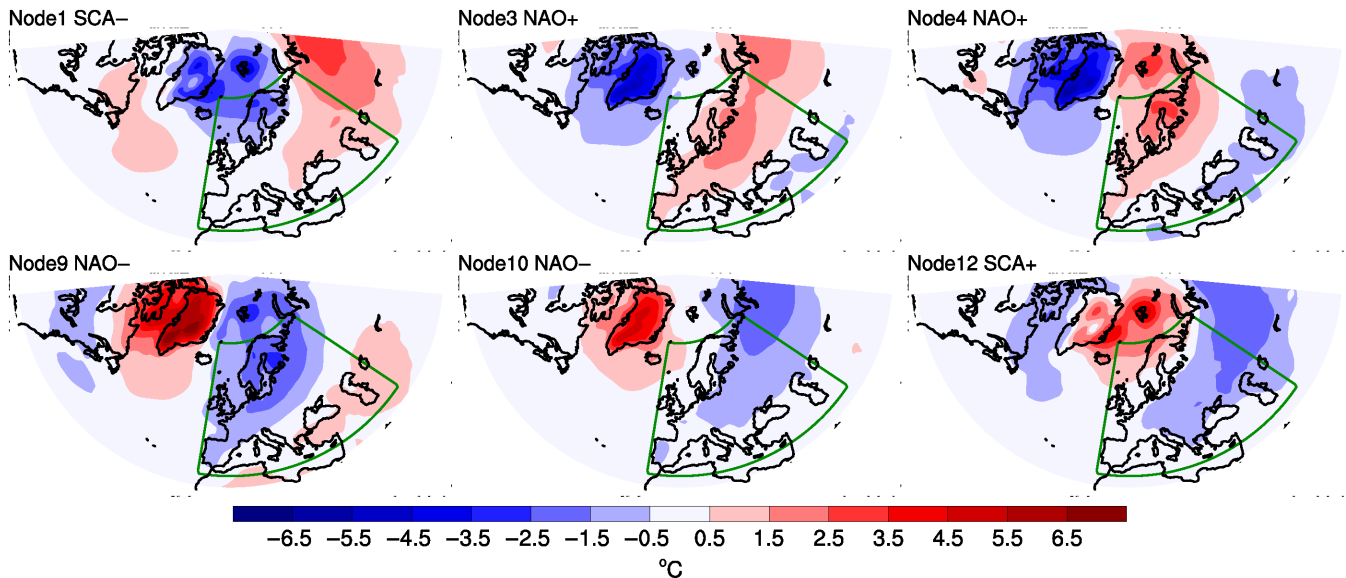
FIGURE 6 2-m temperature anomalies (in °C) for winter (DJFM) in 1979–2015 projected on the same SOM nodes as in Figure 4. The green lines indicate the area 35°–70°N, 10°W–60°E

positive temperature anomalies), whereas the NAO−/Greenland blocking nodes indicate anomalous divergence (favouring negative temperature anomalies). Considering dry-static energy transport, the main differences from these associations are found in southern Europe, where NAO− is associated with anomalous divergence, and in Norway and Iceland, where NAO+ is associated with anomalous divergence. The SCA+ node shows anomalous divergence of latent heat transport over most of Europe, particularly in Scandinavia, whereas the SCA− node is associated with anomalous convergence mostly over Eastern Europe. In contrast, in the case of dry-static energy transport, SCA+ is associated with anomalous convergence in northern Europe, particularly in Scandinavia, and SCA− is associated with anomalous divergence in most of Europe. A quantitative comparison of the resemblance between T2m anomaly patterns and those of the divergence of dry-static energy and latent heat transports is presented in Table 3. The spatial correlation between the time-averaged T2m anomaly and the type of transport divergences over Europe (35°–70°N, 10°W–60°E) depends on the prevailing large-scale circulation. Averaged over cases of NAO− and SCA+, positive

T2m anomalies are collocated with convergence of dry-static energy transport as indicated by high spatial correlation coefficients, but they are weakly or not collocated with convergence of the latent heat transport. In contrast, in conditions of SCA− and NAO+, positive T2m anomalies are better collocated with convergence of latent heat than dry-static energy transport (Table 3). However note that for all nodes shown here, T2m is showing high correlation to the total transport, and except for node 3, the correlations are higher than for the individual components emphasizing the strong linkage between total atmospheric energy transport and local temperature anomalies.

The T2m anomalies related to the most common SOM nodes (Figure 6) are associated with patterns of cold and warm events in various parts of Europe. Cold events in CE and EE (Figure 3) can occur under all 12 SOM nodes, but are most common under SCA− (node 1; Supporting Information Table S1). This is in accordance with large divergence of dry-static energy under SCA- all over WE and CE (Figure 5), which dominates over small convergence of latent heat present in parts of WE and CE (Figure 4). Cold events in NE are most commonly associated with SOM

TABLE 3 Spatial correlation coefficient between energy transport divergence and T2m anomalies in Europe (35°–70°N, 10°W–60°E) for the six most common SOM nodes and for the entire dataset

	Node 1 SCA−	Node 3 Nao+	Node 4 Nao+	Node 9 NAO−	Node 10 NAO−	Node 12 SCA+
Latent heat	−0.48	−0.32	−0.47	−0.31	−0.01	−0.25
Dry-static energy	−0.33	−0.02	−0.28	−0.82	−0.71	−0.63
Total = latent heat + dry-static energy	−0.51	−0.26	−0.53	−0.86	−0.79	−0.81

nodes 1 and 12 (Table S1). This result is interesting, as nodes 1 and 12 correspond to the opposite phases of SCA. However, transport divergence dominates under both phases: latent heat transport mostly diverges over NE for both SCA− and SCA+ (Figure 4), while dry-static energy transport diverges for SCA− but converges for SCA+ (Figure 5). Warm events in WE and NE are in 65–77% of cases associated with SCA+ or NAO+ (node 3, 4, and 12; Table S1). Convergence dominates in this region since for SCA+, divergence of latent heat transport is more than compensated for by convergence of dry-static energy transport, and NAO+ favours strong convergence for latent heat transport, with insignificant signals for dry-static energy. Warm events in SE are more evenly distributed between different SOM nodes, and in EE there has been only a single 4-day-long warm event meeting the 1.75 STD threshold, associated with NAO+, which is strongly associated with convergence of both latent heat and dry-static energy transport.

The NAO+, NAO−, SCA+, and SCA+ nodes are closely associated with both European and Arctic temperature anomalies (Figure 6). Based on detrended data, a statistically significant relationship occurs between SCA− (node 1) and a cold central Arctic (north of 70°N), covering the period from 75 days before to 7 days after the occurrence of SCA− (Figure 7). Analogously, the central Arctic exhibits significant warm anomalies in the period from 4 days before to 6 days after the occurrence of SCA+. However, NAO+ (nodes 3 and 4) is the pattern with the longest and most robust relationship with preceding Arctic winter temperature anomaly: about 90 days of statistically significant cold anomalies in the Arctic precede NAO+ nodes, so that the relationship is stronger for node 3 in days 0–35 and for node 4 in days 36–90. The occurrence of NAO− (nodes 9 and 10) is typically preceded by warm anomalies in the Arctic, but followed by anomalies that vary in sign with a period of approximately a month. This period is typical also for the variability of anomalies related SOM nodes 1, 4, and 12 (Figure 7). The potential causality between Arctic temperature anomalies and successive NAO phase deserves future research.

Comparing winter periods in 1998–2015 and 1979–1997, the SOM nodes show, on average, more warming than cooling, but also coherent areas of cooling are present, although in Europe the cooling is not statistically significant
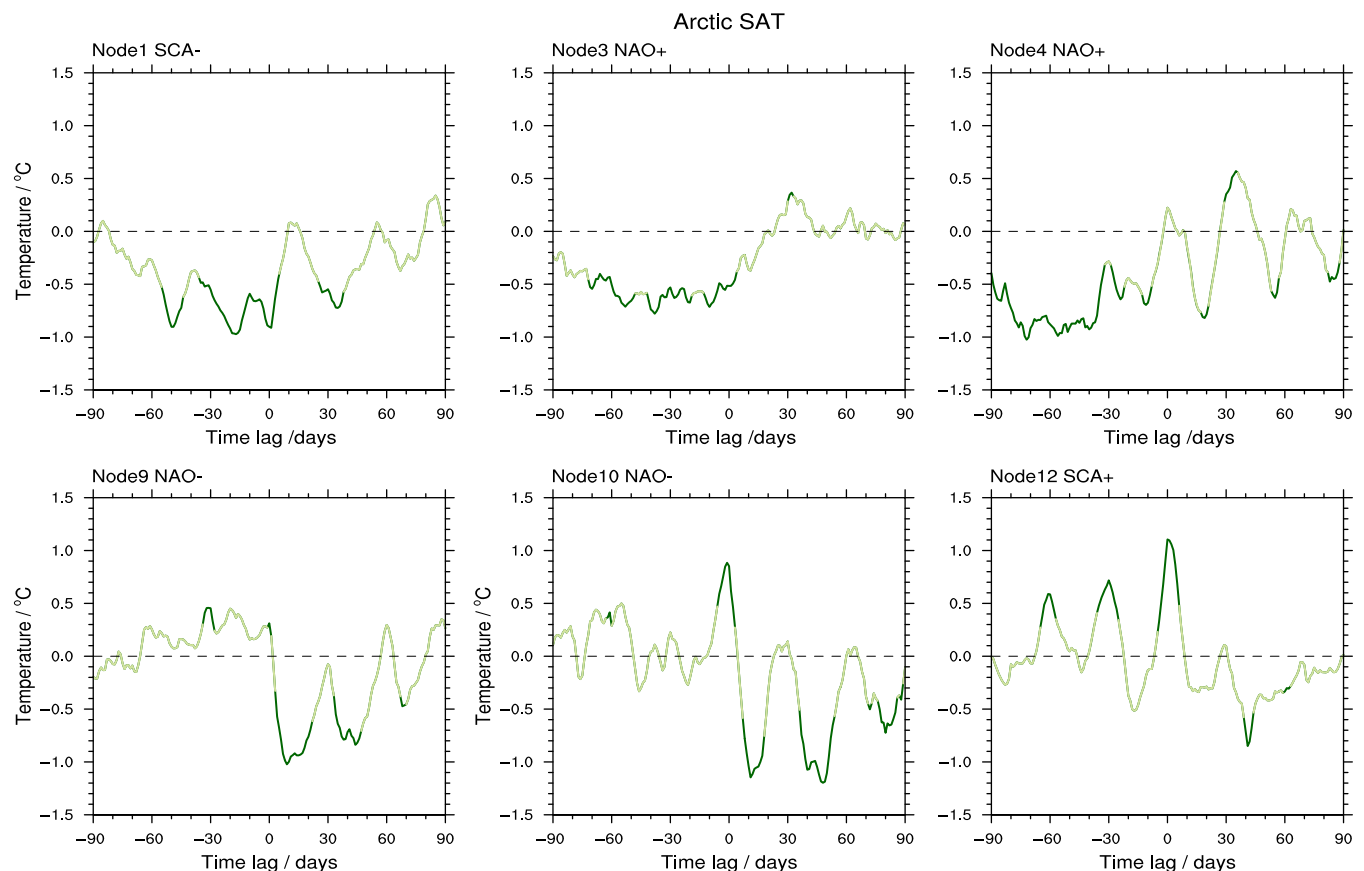

FIGURE 7 Composites of Arctic (north of 70°N) winter (DJFM) detrended 2-m air temperature anomalies as a function of time lag with respect to the six most common large-scale circulation patterns identified by the SOM analysis. Dark lines indicate significance at the 95% confidence level. The significance is determined using a Monte-Carlo approach similar to that applied for Figure 4 [Colour figure can be viewed at wileyonlinelibrary.com]
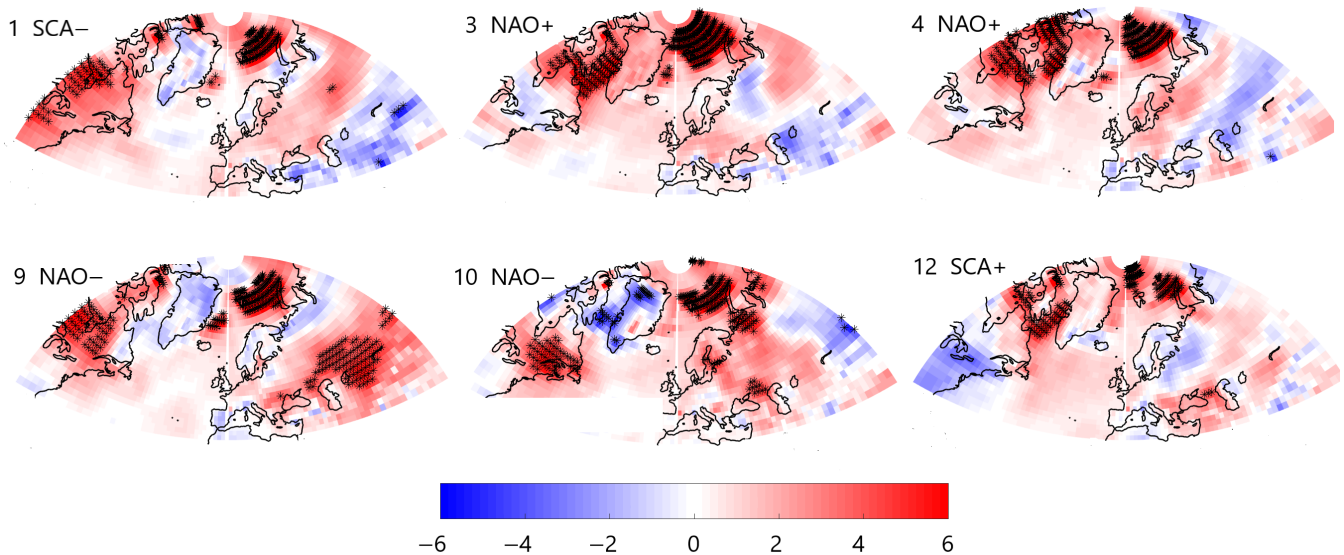
FIGURE 8 Difference in DJFM 2-m temperature anomalies, 1998–2015 minus 1979–1997, for the same SOM nodes as in Figure 4. The black crosses indicate areas with significant values at the 95% confidence level

(Figure 8). Furthermore, the occurrence of some circulation patterns has changed markedly (Figure 9). Considering the entire winter (DJFM), occurrences have decreased for NAO+ ($p < .05$) and SCA− (insignificantly), while they have increased for NAO− ($p < .05$) and SCA+ (insignificantly). The results are qualitatively similar for long-duration events (LDEs, lasting four or more days), for which the winter decrease is significant for node 3 (NAO+) and increase for node 10 (NAO−). However, the changes are not uniform throughout the winter. In December–January, the strongest changes have been the decreased occurrence of SCA− and NAO+ (node 3) and the increased occurrence of NAO− (node 10) and SCA+ (Figure 9). In February and March, the occurrences of NAO+ and SCA+ have decreased while the occurrence of NAO− has increased.

3.2.2 | Results based on cluster analysis

Figure 10 shows five preferred circulation patterns according to cluster analysis, ordered according to their frequency of occurrence, which resemble (1) NAO+ (similar to SOM patterns 3 and 4), (2) the East Atlantic/West Russia pattern (EAWR+) that features high geopotential heights over the North Atlantic and Europe surrounded by negative anomalies, (3) SCA+ (resembling SOM pattern 12), (4) NAO− (resembling SOM patterns 9 and 10), and (5) a strong dipole structure in the east–west direction and positive height anomalies over the Atlantic and Greenland along with negative anomalies over Europe and the Barents Kara Sea (DIPOL, partly resembling SOM patterns 1 and 5). Comparing periods 1998–2015 and 1979–1997, there are statistically significant increases in the frequency of occurrence of

SCA+ in December and January and in the frequency of occurrence of NAO− in March (and in February at 90% significance level). In addition, blocking over the North Atlantic (DIPOL, in February) and in late winter over the British Isles/North Sea (EAWR+, in March) occurred significantly more frequently during 1998–2015. Accordingly, the results in Figure 10 support conclusions based on the SOM analysis in Figure 9.

Next we compare T2m anomalies for each SOM node (Figure 6) and for each pattern revealed by the cluster analysis (Figure S1). Considering NAO−, T2m anomalies based on the SOM and cluster methods are qualitatively similar, but in Central Europe the cluster analysis reveals anomalies that are not as cold as those in the SOM analysis. Also, the positive anomalies in the Greenland–Baffin region are located farther west in the cluster results. Both negative and positive T2m anomalies related to NAO+ are somewhat stronger in the SOM-based results, but in the Barents and Greenland seas the differences between the two SOM nodes associated with NAO+ (nodes 3 and 4) are larger than the differences between SOM- and cluster-based results. For SCA+, SOM analysis yields stronger T2m anomalies in Central Europe and Greenland. The SOM-cluster analysis differences reported above are due to the differences in the population of Z500 fields belonging to certain SOM nodes and clusters (compare Figures 2 and 10). The more extreme negative and positive T2m anomalies based on SOM analysis are due to the six most common SOM nodes representing 66% of the daily data from 1979 to 2015, whereas the five clusters together cover all the data. The cluster analysis reveals the EAWR and DIPOL patterns and the associated T2m anomaly fields, such as the European warm anomalies
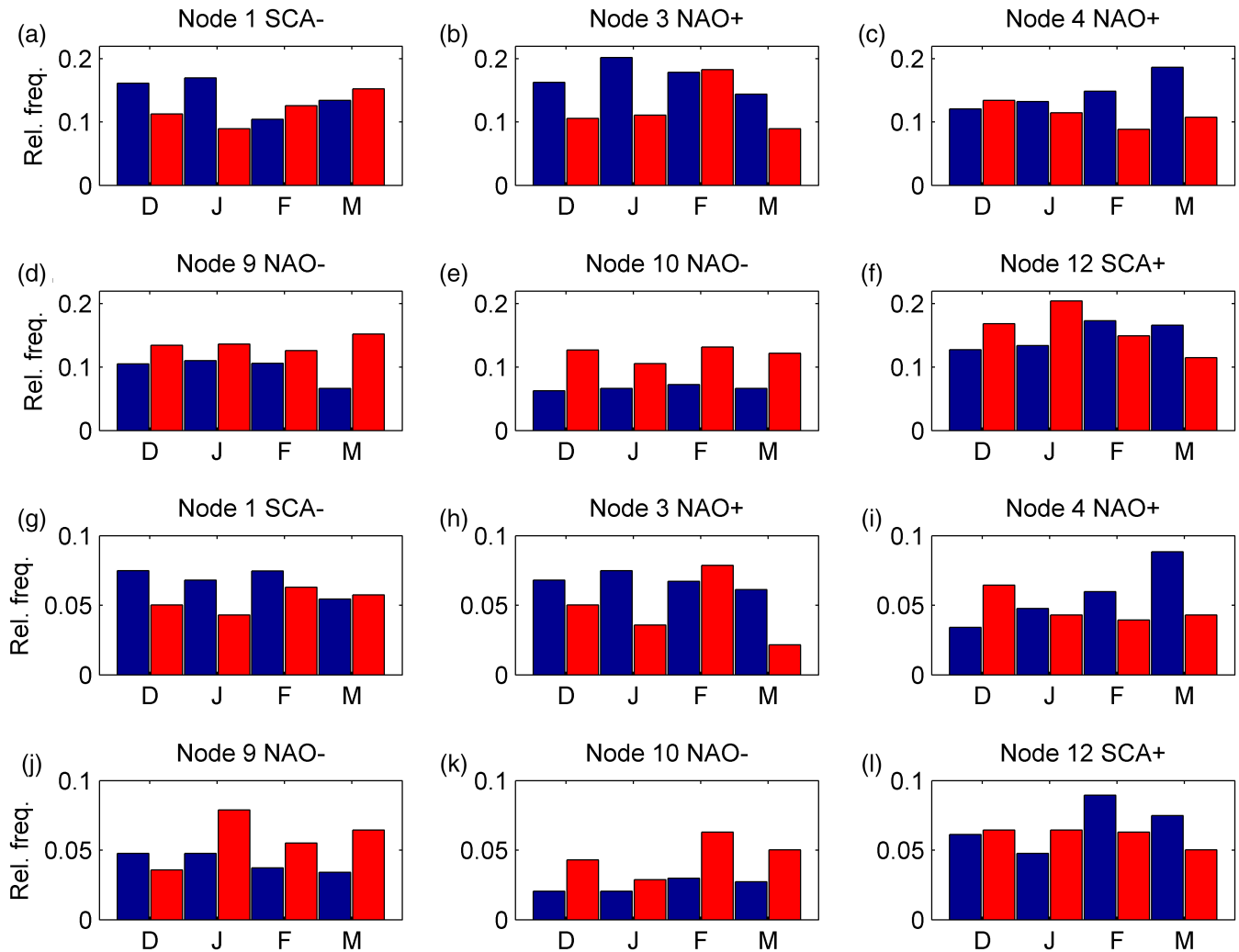
FIGURE 9 Histograms for the monthly (DJFM) relative frequency of occurrence of the same SOM nodes as in Figure 4 for (a–f) all events and (g–l) solely for cases when the atmosphere has resided in the same pattern for at least four consecutive days. The blue and red bars are for the periods 1979–1997 and 1998–2015, respectively

solely in Scandinavia and Iceland under EAWR and solely in Russia under DIPOL, which are not present in the SOM-based results. Hence, application of the two analysis methods is complementary, and reveals information on the sensitivity of the results to the method applied, and perhaps the differing spatial domains of the analyses. Both results are naturally somewhat sensitive to the number of patterns pre-selected.

Considering T2m changes between 1979–1997 and 1998–2015, results based on SOM (Figure 8) and cluster (Figure S2) analyses are qualitatively similar, but include the following differences. For the patterns that resemble NAO+, the cluster analysis shows warming almost everywhere, but the SOM analysis also reveals regions of cooling, for example, to the east and northeast of the Caspian Sea. For NAO- the largest differences occur in Greenland, with cooling based on SOM analyses and warming based on cluster

analyses. For SCA+ the European cooling is shifted farther northeast in the cluster-based results.

Although the analyses presented in this sub-section do not prove causality, the results are similar to those obtained by Crasemann *et al.* (2017), who carried out atmospheric general circulation model sensitivity experiments for different prescribed Arctic sea-ice conditions. The modelled increase in the frequency of occurrence of SCA+ and NAO− for low sea-ice conditions were similar to those detected from ERA-Interim, suggesting that the increased occurrences can be attributed to changes in Arctic sea-ice conditions.

3.3 | Airmass transport to Europe

Changes in the occurrence of large-scale circulation patterns and the air temperatures associated with each pattern are
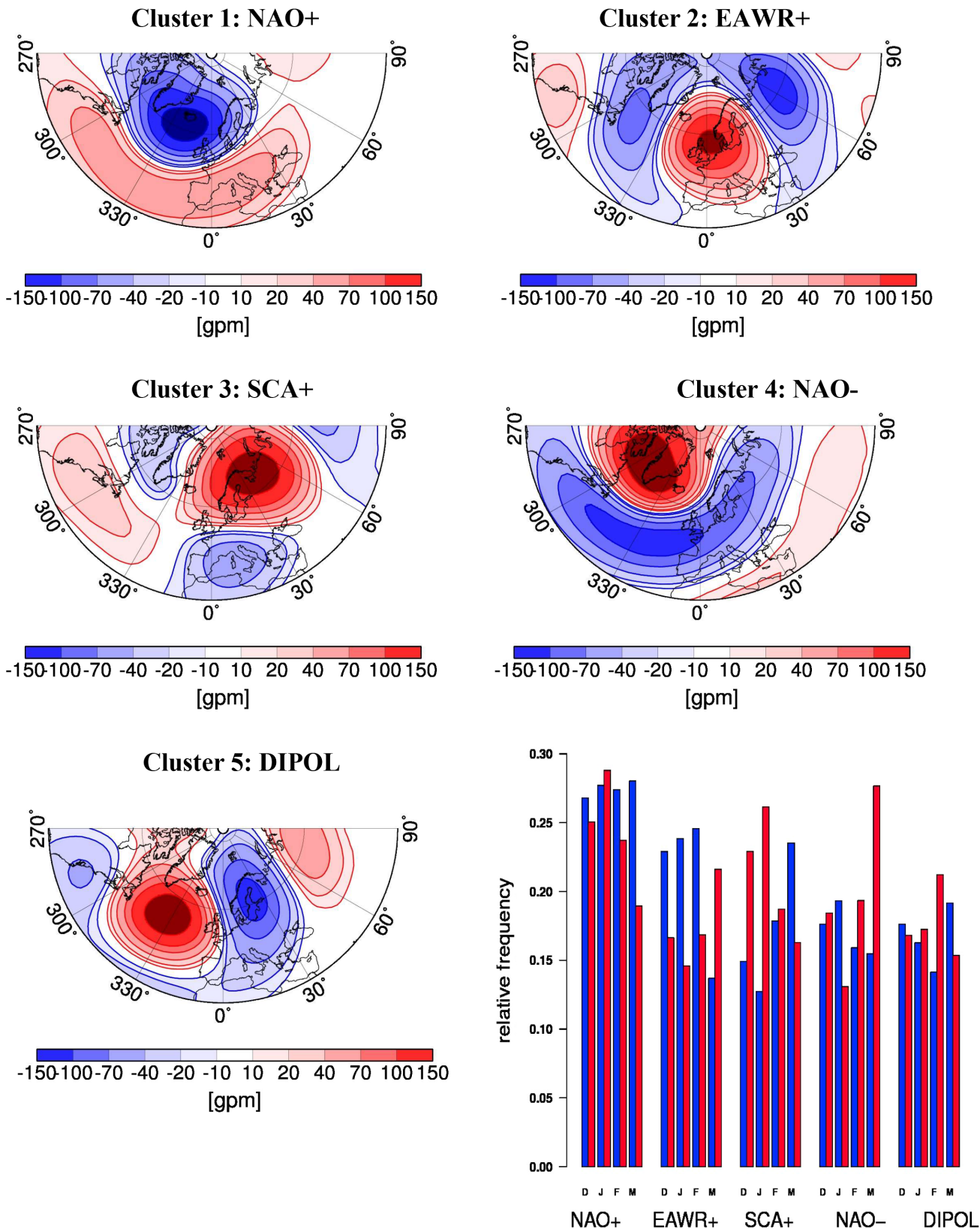
FIGURE 10 Geopotential anomalies at 500 hPa for the five most common large-scale patterns obtained by a cluster analysis using winter (DJFM) ERA-interim data. Histogram shows the relative monthly frequency of occurrence of each cluster, where blue and red bars are for the periods 1979–1997 and 1998–2015

expected to be reflected in the temperatures of airmasses of different origin transported to Europe, which motivated us to analyse airmass trajectories.

Among the 10 selected cities (Section 2.3), the daily occurrence of air masses with Arctic (here defined as north of 70°N) origin varied from 4% in Rome to 40% in Hammerfest. Comparing the period 1998–2015 against 1979–1997, in all 10 cities the occurrence of Arctic-origin airmasses has remained essentially the same, and the temperatures of Arctic-origin air have increased on average by 0.5°C. This equals the temperature increase averaged over all airmass origins for the 10 cities. However, the warming under Arctic-origin air has not been uniform throughout the winter: in Archangelsk, Hammerfest, Helsinki, Kazan, Minsk, and Berlin, the temperatures have increased in December and January but decreased in March. The early-winter warming has been strongest in Hammerfest and Minsk (1.8°C) and the March cooling has been strongest in Helsinki and Archangelsk (−1.5°C). Airmasses of Arctic origin occur under all five circulation patterns based on the cluster analyses, but they are most common in the NAO− pattern (24% of cases), and least common in the SCA+ pattern (11%).

We next focus on the direction instead of the latitude of airmass origin. In cases of airmasses coming from the northeast, northwest, or southwest, the period 1998–2015 has been warmer than the period 1979–1997 in all 10 cities (Figure 11). However, in cases of southeasterly airmass origin, cooling occurred in the eastern-most cities of Kazan (−1.0°C), Moscow (−0.8°C), Helsinki (−0.7°C), and Archangelsk (−0.5°C). If the general warming trend (averaged over all airmass origins) is removed from the time series, the cooling is significant ($p < .01$) in Kazan, Helsinki, and Moscow.

The winter cooling in cases of southeasterly airmass origin was associated with changes in the occurrence of different large-scale circulation patterns (Table 4) and with the mean temperature and its change under each pattern (Figure 12). We identify the change in a pattern occurrence as the dynamic effect, and the change in the mean temperature of a pattern as the thermodynamic effect. The dynamical factors associated with a southeasterly airmass origin are as follows. In the four eastern-most cities (Archangelsk, Helsinki, Kazan, and Moscow), NAO− is associated with the lowest or second-lowest (in Kazan) air temperature (Figure 12a), and the NAO- pattern has become increasingly common (Table 4). In contrast, the occurrence of NAO+, which is the warmest or second-warmest (in Archangelsk) pattern, has strongly decreased. Further, in Archangelsk the cooling is also related to the slightly increased occurrence of the rather cold DIPOL pattern. Thermodynamic factors also contributed to the cooling: cooling of the DIPOL pattern in Archangelsk and cooling of the SCA+ pattern in Kazan (see

also Figure 8). The following factors opposed the cooling but did not dominate over it: thermodynamic warming of the NAO+ and NAO− patterns in all four cities, and an increased occurrence (dynamic factor) of the warm SCA+ pattern in Kazan (Figure 12, Table 4).

As in the case of temperature changes for Arctic airmass origin, the cooling in cases of southeasterly airmass origin has not been uniform throughout the winter. The winter averages are dominated by cooling during March in Kazan, Archangelsk, and Moscow, with monthly mean values of −1.8, −1.3, and − 0.8 K, respectively. As was the case for the entire winter, we find that during March the principal dynamic effect responsible for cooling in all three cities, is the significantly increased occurrence of NAO− (Table S2). The other dynamic effects are as follows. In Kazan in March, the DIPOL pattern is warm, and its occurrence has strongly decreased. In Archangelsk, SCA+ and NAO+ are the warmest patterns, and their occurrences have decreased. In Moscow, NAO+ is the warmest pattern with a decreased occurrence.

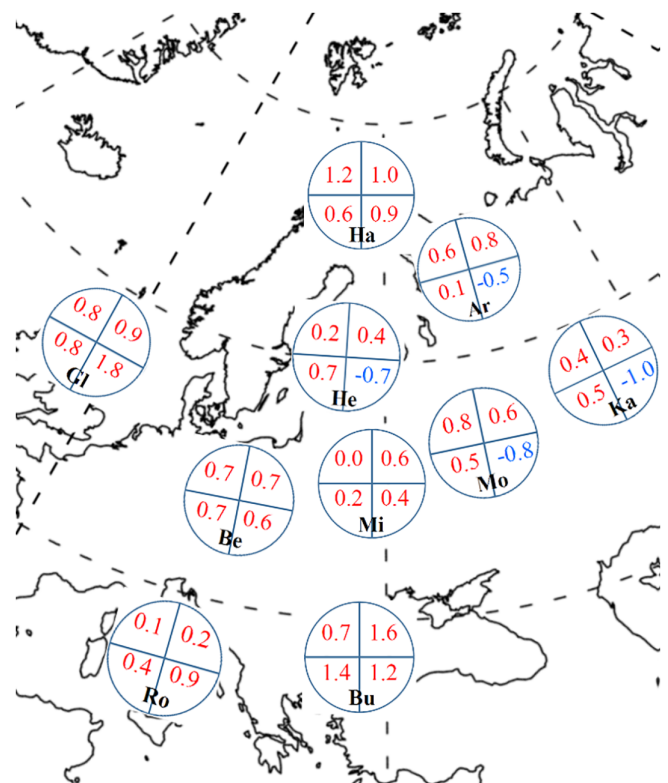**FIGURE 11** Differences in winter (DJFM) mean air temperature (°C) at 1 km height between the periods 1998–2015 and 1979–1997 in cases of airmass origins in the northwest, northeast, southeast, and southwest (noted in corresponding quadrants of circles) for Archangelsk (Ar), Berlin (be), Bucharest (Bu), Glasgow (Gl), Hammerfest (ha), Helsinki (he), Kazan (Ka), Minsk (mi), Moscow (Mo), and Rome (Ro)

TABLE 4 Occurrence (in %) of large-scale circulation patterns, based on cluster analysis, in conditions of airmass origins from the southeast (SE), southwest (SW), and northeast (NE) for selected cities

Origin	City	C1 = NAO+		C2 = EAWR		C3 = SCA+		C4 = NAO-		C5 = DIPOL	
		1979–1997	1998–2015	1979–1997	1998–2015	1979–1997	1998–2015	1979–1997	1998–2015	1979–1997	1998–2015
SE	Hel	15	10	7	8	40	45	21	26	16	11
SE	Arc	22	14	11	13	29	31	22	25	16	18
SE	Kaz	28	18	7	6	28	37	15	21	22	17
SE	Mos	21	13	8	7	38	39	17	23	16	17
SE	Gla	7	5	30	36	25	24	29	29	8	6
SE	Buc	12	11	19	12	35	42	20	12	14	13
SW	Buc	34	33	18	12	11	16	22	23	15	17
NE	Buc	16	13	22	25	33	28	15	19	14	16
NE	Ham	23	18	25	15	8	10	27	29	18	27
NW	Ham	24	22	22	19	12	13	20	20	22	26

Common changes in Archangelsk, Helsinki, Kazan, and Moscow were (a) a decrease of subsidence along the airmass trajectories (Figure S3) and, as a smaller effect, (b) low-tropospheric cooling at the trajectory starting points. Averaged over the four cities, the mean height of the starting points of the trajectories was 1,750 m in 1979–1997 but only 1,480 m in 1998–2015. Applying Equation (3) we found out that during 1998–2015 there was on average 2.6°C less adiabatic subsidence heating during the 5-day airflow. This alone would have caused an even larger temperature decrease than observed in the four cities (Figure 11), but diabatic heating/cooling processes were also active during the transport.

An important diabatic process is cloud radiative effect. We analysed four relevant variables: total column liquid water, total column ice, total column water (sum of vapour, liquid, and ice), and total cloud fraction (including low-, middle-, and high-level clouds) over Helsinki, Kazan, Moscow, and Archangelsk. Comparing the periods 1979–1997 and 1998–2015, there are predominantly increasing values for all these variables both when averaged over all airmass origins and when calculated separately for southeasterly airmass origins (Table S3). As subsidence typically favours reduced cloud cover (van der Dussen et al., 2016), the results for increased cloudiness are consistent with the decreased subsidence in cases of southeasterly airmass origin. Note that we address air temperatures at 1 km altitude. Hence, there is not such a marked wintertime warming effect of clouds via increased downward longwave radiation as there would be at the surface. For airmass origins other than southeasterly and for the Arctic origins (north of 70°N), the changes in adiabatic subsidence heating were small.

In addition to the anomalous cooling cases, the strongest warmings for certain airmass origins deserve attention (Figure 11). In Glasgow, the airmasses of southeasterly origin have become 1.8°C warmer. This is due to both thermodynamic and dynamic effects: warming under all circulation patterns and an increased occurrence of the warmest pattern, EAWR (with a 500 hPa high over British Isles), during southeasterly flow (Figure 12; Table 4). In Hammerfest, warming has been strongest in cases of northwesterly and northeasterly airmass origins. This is mostly related to overall warming during NAO−, EAWR, NAO+, and DIPOL (Figure 12), which has dominated over the effects of increasing occurrence of the cold NAO− and DIPOL patterns (Table 4). Also the occurrence of the relatively warm SCA+ pattern has increased during northeasterly and northwesterly flows. The strongest overall warming has occurred in Bucharest (Figure 11), where all five patterns have become warmer (Figure 12). Considering dynamical effects, during southeasterly flows the strongly increased occurrence of the by far warmest NAO+ pattern has dominated. During southwesterly flows, the decreased occurrence of the cold EAWR
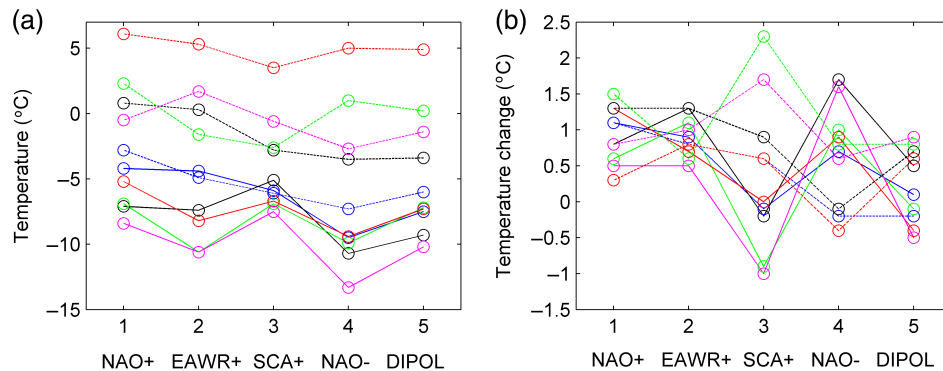
FIGURE 12 (a) Winter (DJFM) mean air temperature at 1 km height over the selected cities during 1979–2015 for the five circulation patterns identified on the basis of cluster analysis, and (b) the temperature difference between periods 1998–2015 and 1979–1997, for Helsinki (blue solid lines), Hammerfest (black solid lines), Kazan (green solid lines), Moscow (red solid lines), Archangelsk (magenta solid lines), Minsk (blue dashed lines), Berlin (black dashed lines), Bucharest (green dashed lines), Rome (red dashed lines), and Glasgow (magenta dashed lines)

pattern has contributed to warming. In contrast, the occurrence of the even colder SCA+ pattern has increased, but its effect has been partly compensated by the strong thermodynamic warming of the pattern. During northeasterly flows, dynamic effects supporting warming include the decreased occurrence of the cold SCA+ pattern and increased occurrence of NAO−, which is associated with high temperatures in Bucharest.

4 | DISCUSSION AND CONCLUSIONS

Our study investigated multiple approaches to illuminate the factors contributing to regional temperature variations in Europe, how temperatures are changing in the recent era of Arctic amplification, and which factors are responsible for the changes. Analysis methods include spatial and lagged correlations, two types of pattern analysis, back trajectories of airmass origins, and a separation of dynamic and thermodynamic contributions to temperature changes.

The analyses revealed several new quantitative findings for the spatial relationship between regional temperature variations in Europe and the Arctic, summarized in the five points below:

1. Statistical relationships between the number of cold days in CE and NE and warm days in Greenland have become consistently stronger during the AA era, as have relationships between cold days in SE and EE and warm days in the Barents–Kara seas region (Table 2).

Extreme cold winter events, at least 4 days long, in WE, CE, and NE are significantly related to positive temperature anomalies in the Greenland/Baffin region, whereas in SE and EE extremely cold winter events are associated with both the Greenland/Baffin region and the Barents–Kara seas

area (Figure 3). In addition, inter-annual variations in Europe are associated with those in the Arctic, seen as significant correlations between the number of cold days per winter in Europe and the number of warm days per winter in the Arctic (Table 2), with basically the same geographic relationships between the European and Arctic regions as in the case of synoptic-scale extreme events. Both the synoptic-scale (Table 1) and inter-annual (Table 2) relationships are stronger during the period of AA. While these results do not prove causality, they are qualitatively consistent with previous results suggesting that AA favours cold winter events in mid-latitudes, including Europe (Yang and Christensen, 2012; Grassi *et al*., 2013; Cohen *et al*., 2014; Koenigk *et al*., 2016; Screen, 2017).

The large-scale circulation analyses, based on SOM and cluster methods, demonstrated close associations of both NAO and SCA with European winter temperatures (Figures 6 and 10), in line with previous studies (e.g., Yiou and Nogaj, 2004). The cluster method also highlighted the role of EAWR and DIPOL patterns.

2. Under the occurrence of NAO− and SCA+, European temperature anomalies were mostly collocated with convergence of dry-static energy transport, whereas under NAO+ and SCA− the temperature anomalies were to some extent collocated with convergence of latent heat transport (Table 3).

We interpret these relationships to mean that NAO+ and SCA− are associated with stronger westerly winds that advect moist airmasses from the Atlantic to Europe, resulting in a strong effect of latent heat transport on T2m. In contrast, NAO− and SCA+ favour more meridional circulation types, during which dry-static energy transport dominates. Also, under NAO− and SCA+, European winter temperatures are typically low (Figure 6), which limits the maximum possible latent heat content of the airmass. Spatial

correlations between T2m anomalies and the sum of latent heat and dry-static energy convergences are in most cases strongly negative, but do not reach −1, as T2m anomalies are also affected by local factors not controlled by large-scale transport. Although the magnitude of latent heat transport divergence is mainly smaller than that of the dry-static energy transport divergence, it sometimes, mostly under NAO− and SAC+, has a larger effect on near-surface temperatures, as the latent heat transport also enhances the local greenhouse effect by increasing the local humidity and cloudiness (Graversen and Burtu, 2016).

3. The statistically significant lagged relationships between detrended Arctic temperature anomalies and large-scale circulation patterns (Figure 7) was an important finding. The most robust result was that SCA− and NAO+ are typically preceded by a long period, up to 3 months, of negative temperature anomaly averaged over the circumpolar Arctic north of 70°N.

As NAO+ and SCA− on average coincide with a strong zonal flow (Bueh and Nakamura, 2007; Hurrell and Deser, 2009), this result aligns with previous findings that AA is associated with weaker zonal winds (Francis and Vavrus, 2012, 2015; Davy et al., 2018). Interestingly, there is a more robust relationship between Arctic temperature anomalies and NAO/SCA patterns (longer and more continuous periods of statistically significant temperature anomalies) in the case of an abnormally cold Arctic at time scales of 1 to 90 days than in the case of a warm Arctic, which has received more attention as AA has intensified (Pedersen et al., 2016; Vavrus, 2018). The results presented in Figure 7 can be exploited to improve seasonal forecasting, an endeavour that warrants further study.

4. Comparing periods 1998–2015 and 1979–1997, both the SOM and cluster methods indicated statistically significant increases in the occurrence of SCA+ in December and January and NAO− in February and March. In general, SCA+ and NAO− favour cold winter weather in Europe.

The changes observed are potentially associated with the sea-ice decline in the Barents and Kara seas, favouring SCA+ in early winter (Jaiser et al., 2012; Crasemann et al., 2017), and enhancement of the climatological planetary wavenumber 1 through constructive wave interference (Smith et al., 2010; Hoshi et al., 2019 and references therein). According to Jaiser et al. (2013, 2016), this process is followed by an increased flux of wave activity propagating to the stratosphere, which may finally lead to a tropospheric Arctic Oscillation response through downward stratosphere-to-troposphere coupling mechanisms, further strengthening the Siberian high (Cohen et al., 2014; Kidston et al., 2015). The Arctic Oscillation response manifests over the North Atlantic-Eurasian region as an increased frequency of occurrence of NAO- in late winter. Some modelling studies have suggested that the strengthening of the Siberian high is due to inter-annual and decadal variability (McCusker et al., 2016), but experiments applying models with a well-resolved stratosphere show a robust link with AA (Wu and Smith, 2016; Zhang et al., 2019).

5. Comparing periods 1979–1997 and 1998–2015, in cases of southeasterly airmass origin, cooling at 1 km altitude occurred in Kazan, Moscow, Helsinki, and Archangelsk, in particular in March.

In these cities, a major contributing cooling effect was the decrease of subsidence along the airmass trajectories. Considering horizontal large-scale circulation, the cooling was associated with dynamic factors (changes in pattern frequency) that dominated over the overall thermodynamic (pattern-wide) warming. Circulation patterns associated with low temperatures, particularly the NAO- and related southeasterly flow, became more common during 1998–2015, while patterns associated with high temperatures, particularly NAO+, became rarer. The winter-average T2m change in Kazan, Archangelsk, and Moscow was dominated by cooling in March, with monthly mean values of −1.8, −1.3, and − 0.8 K, respectively. This cooling was due primarily to the significantly increased occurrence of NAO- (dynamic effect). These results are consistent with the previously discussed strengthening of the Siberian high in March. In general, our results are in accordance with previous studies demonstrating the major role of dynamic effects in decadal-scale variations in mean and extreme air temperatures (Corti et al., 1999; Yiou and Nogaj, 2004).

During the period of recent AA, airmasses originating from the Arctic have, by definition, become generally warmer. However, Arctic warming has also indirectly affected Europe in winter. An increased frequency in long-duration events associated with NAO− (Figure 9j,k) favours persistent cold winter weather in Europe, and a decrease of those events, associated with NAO+, favours less persistent warm winter periods. An increased persistence is favoured by the finding that NAO− patterns have increased more than NAO+ patterns.

Notwithstanding, comparing the period 1998–2015 against 1979–1997, European winters have generally warmed (Figures 8, 11, and 12b; Figure S2).

Finally, we acknowledge that European winter temperatures are also affected by other factors than those explicitly discussed above. Such factors include atmosphere–ocean coupling in the tropics and subtropics; shifting large-scale ocean temperature patterns; radiative forcings by greenhouse gases, aerosols, and ozone; as well as internal variability. The projected future amplification of climate warming in the upper tropical troposphere would tend to strengthen the subtropical jet stream and shift it farther north, acting against

the effects of Arctic amplification (McGraw and Barnes, 2016; Zappa *et al.*, 2018). In addition, many studies have identified linkages between SST variations in the tropical and/or northern Atlantic Ocean and weather patterns in Europe (Marshall *et al.*, 2001b; Cassou *et al.*, 2004; Sato *et al.*, 2014; Davini *et al.*, 2015; Hall *et al.*, 2015; Yeager and Robson, 2017). Furthermore, the Pacific Decadal Oscillation (PDO) potentially has remote effects on European winters (Trenberth and Fasullo, 2013; Vihma *et al.*, 2014). On multi-decadal time scales, the Atlantic Multi-decadal Variability (AMO) also plays important role (Keenlyside and Omrani, 2014; Peings and Magnusdottir, 2014). In any case, the effects of all factors, except the direct radiative forcing, are implicitly included in the reanalysis-based large-scale circulation patterns objectively analysed here.

North Atlantic variability will dominate the day-to-day and year-to-year fluctuations in future European winter temperatures. However, as greenhouse gases accumulate further and Arctic amplification intensifies, our findings suggest that Arctic influences on European winter weather may intensify, perhaps leading to more unusual and persistent weather events.

ORCID

Timo Vihma https://orcid.org/0000-0002-6557-7084
Linling Chen https://orcid.org/0000-0002-7865-9177
Richard Hall https://orcid.org/0000-0003-4840-383X
Edward Hanna https://orcid.org/0000-0002-8683-182X
James E. Overland https://orcid.org/0000-0002-2012-8832

REFERENCES

Barnston, A.G. and Livezey, R.E. (1987) Classification, seasonality and persistence of low frequency atmospheric circulation patterns. *Monthly Weather Review*, 115, 1083–1126.

Bojariu, R. and Reverdin, G. (2002) Large-scale variability modes of freshwater flux and precipitation over the Atlantic. *Climate Dynamics*, 18, 369–381.

Buckley, M.W. and Marshall, J. (2016) Observations, inferences, and mechanisms of Atlantic meridional overturning circulation variability: a review. *Reviews of Geophysics*, 54, 5–63. https://doi.org/10.1002/2015RG000493.

Bueh, C. and Nakamura, H. (2007) Scandinavian pattern and its climate impact. *Quarterly Journal of the Royal Meteorological Society*, 133, 2117–2131.

Cassou, C., Terray, L., Hurrell, J.W. and Deser, C. (2004) North Atlantic winter climate regimes: spatial asymmetry, stationarity with time, and oceanic forcing. *Journal of Climate*, 17, 1055–1068.

Cohen, J., et al. (2014) Recent Arctic amplification and extreme mid-latitude weather. *Nature Geoscience*, 7, 627–637. https://doi.org/10.1038/ngeo2234.

Cohen, J., Francis, J.A. and Pfeiffer, K. (2017) A turning point in ENSO-based seasonal forecasts. *Oceanography*, 30(1), 115.

Cohen, J., Pfeiffer, K. and Francis, J.A. (2018) Warm Arctic episodes linked with increased frequency of extreme winter weather in the United States. *Nature Communications*, 9, 869.

Corti, S., Molteni, F. and Palmer, T.N. (1999) Signature of recent climate change in frequencies of natural atmospheric circulation regimes. *Nature*, 398, 799–802.

Coumou, D., Petoukhov, V., Rahmstorf, S., Petri, S. and Schellnhuber, H.-J. (2014) Quasi-resonant circulation regimes and hemispheric synchronization of extreme weather in boreal summer. *Proceedings of the National Academy of Sciences of the United States of America*, 111(34), 12331–12336.

Crasemann, B., Handorf, D., Jaiser, R., Dethloff, K., Nakamura, T., Ukita, J. and Yamazaki, K. (2017) Can preferred atmospheric circulation patterns over the North-Atlantic-Eurasian region be associated with arctic sea ice loss? *Polar Science*, 14, 9–20.

Davini, P., von Hardenberg, J. and Corti, S. (2015) Tropical origin for the impacts of the Atlantic multidecadal variability on the euro-Atlantic climate. *Environmental Research Letters*, 10, 094010.

Davy, R., Chen, L. and Hanna, E. (2018) Arctic amplification metrics. *International Journal of Climatology*, 38, 4384–4394.

Dawson, A. and Palmer, T.N. (2015) Simulating weather regimes: impact of model resolution and stochastic parameterization. *Climate Dynamics*, 44, 2177–2193.

Dee, D.P., Uppala, S.M., Simmons, A.J., Berrisford, P., Poli, P., Kobayashi, S., Andrae, U., Balmaseda, M.A., Balsamo, G., Bauer, P., Bechtold, P., ACM, B., van de Berg, L., Bidlot, J., Bormann, N., Delsol, C., Dragani, R., Fuentes, M., Geer, A.J., Haimberger, L., Healy, S.B., Hersbach, H., Hólm, E.V., Isaksen, L., Kållberg, P., Köhler, M., Matricardi, M., McNally, A.P., Monge-Sanz, B.M., Morcrette, J.-J., Park, B.-K., Peubey, C., de Rosnay, P., Tavolato, C.,

Thépaut, J.-N. and Vitart, F. (2011) The ERA-interim reanalysis: configuration and performance of the data assimilation system. *Quarterly Journal of the Royal Meteorological Society*, 137, 553–597.

Deser, C., Sun, L., Tomas, R.A. and Screen, J. (2016) Does ocean coupling matter for the northern extratropical response to projected Arctic Sea ice loss? *Geophysical Research Letters*, 43, 2149–2157.

van der Dussen, J.J., de Roode, S.R. and Siebesma, A.P. (2016) How large-scale subsidence affects stratocumulus transitions. *Atmospheric Chemistry and Physics*, 16, 691–701.

Francis, J.A. (2017) Why are Arctic linkages to extreme weather still up in the air? *Bulletin of the American Meteorological Society*, 98, 2551–2557.

Francis, J.A. and Skific, N. (2015) Evidence linking rapid Arctic warming to mid-latitude weather patterns. *Philosophical Transactions of the Royal Society A*, 373, 20140170. https://doi.org/10.1098/rsta.2014.0170.

Francis, J.A. and Vavrus, S.J. (2012) Evidence linking Arctic amplification to extreme weather in mid-latitudes. *Geophysical Research Letters*, 39, L06801.

Francis, J.A. and Vavrus, S.J. (2015) Evidence for a wavier jet stream in response to rapid Arctic warming. *Environmental Research Letters*, 10, 014005.

Francis, J.A., Skific, N. and Vavrus, S.J. (2018) North American weather regimes are becoming more persistent: is Arctic amplification a factor? *Geophysical Research Letters*, in review, 45, 11,414–11,422.

Grassi, B., Redaelli, G. and Visconti, G. (2013) Arctic Sea-ice reduction and extreme climate events over the Mediterranean region. *Journal of Climate*, 26, 10101–10110. https://doi.org/10.1175/JCLI-D-12-00697.1.

Graversen, R.G. (2006) Do changes in mid-latitude have any impact on the Arctic surface air temperature trend? *Journal of Climate*, 19, 5422–5438.

Graversen, R.G. and Burtu, M. (2016) Arctic amplification enhanced by latent energy transport of atmospheric planetary waves. *Quarterly Journal of the Royal Meteorological Society*, 142, 2046–2054.

Hall, R., Erdélyi, R., Hanna, E., Jones, J.M. and Scaife, A.A. (2015) Drivers of North Atlantic polar front jet stream variability. *International Journal of Climatology*, 35, 1697–1720. https://doi.org/10.1002/joc.4121.

Handorf, D., Jaiser, R., Dethloff, K., Rinke, A. and Cohen, J. (2015) Impacts of Arctic Sea ice and continental snow cover changes on atmospheric winter teleconnections. *Geophysical Research Letters*, 42, 2367–2377. https://doi.org/10.1002/2015GL063203.

Hanna, E., and T.E. Cropper (2017) North Atlantic Oscillation. Oxford Research Encyclopedia of Climate Science, http://climatescience.oxfordre.com/view/10.1093/acrefore/9780190228620.001.0001/acrefore-9780190228620-e-22

Hanna, E., Cropper, T.E., Hall, R.J. and Cappelen, J. (2016) Greenland blocking index 1851–2015: a regional climate change signal. *International Journal of Climatology*, 36, 4847–4861.

Hanna, E., Hall, R.J. and Overland, J.E. (2017) Can Arctic warming influence UK extreme weather? *Weather*, 72, 346–352.

Hanna, E., Hall, R.J., Cropper, T.E., Ballinger, T.J., Wake, L., Mote, T. and Cappelen, J. (2018) Greenland blocking index daily series 1851-2015: analysis of changes in extremes and links with North Atlantic and UK climate variability and change. *International Journal of Climatology*, 38, 3546–3564.

Hewitson, B. and Crane, R. (2002) Self-organizing maps: applications to synoptic climatology. *Climate Research*, 22(1), 13–26.

Hoshi, K., Ukita, J., Honda, M., Nakamura, T., Yamazaki, K., Miyoshi, Y. and Jaiser, R. (2019) Weakstratospheric polar vortex events modulated by the Arctic Sea-ice loss. *Journal of Geophysical Research: Atmospheres*, 124, 858–869. https://doi.org/10.1029/2018JD029222

Hurrell, J.W. and Deser, C. (2009) North Atlantic climate variability: the role of the North Atlantic oscillation. *Journal of Marine Systems*, 78, 28–41.

Hurrell, J.W., Kushnir, Y., Ottersen, G. and Visbeck, M. (2003). An overview of the North Atlantic oscillation, 134, American Geophysical Union.

IPCC. (2012) Managing the risks of extreme events and disasters to advance climate change adaptation. In: Field, C.B., Barros, V., Stocker, T.F., Qin, D., Dokken, D.J., Ebi, K.L., Mastrandrea, M.D., Mach, K.J., Plattner, G.-K., Allen, S.K., Tignor, M. and Midgley, P.M. (Eds.) *A Special Report of Working Groups I and II of the Intergovernmental Panel on Climate Change*. Cambridge and New York: Cambridge University Press, p. 582.

Jaiser, R., Dethloff, K., Handorf, D., Rinke, A. and Cohen, J. (2012) Impact of sea ice cover changes on the Northern Hemisphere atmospheric winter circulation. *Tellus A: Dynamic Meteorology and Oceanography*, 64, 11595. https://doi.org/10.3402/tellusa.v64i0.11595.

Jaiser, R., Dethloff, K. and Handorf, D. (2013) Stratospheric response to Arctic sea ice retreat and associated planetary wave propagation changes. *Tellus A: Dynamic Meteorology and Oceanography*, 65, 19375. https://doi.org/10.3402/tellusa.v65i0.19375.

Jaiser, R., Nakamura, T., Handorf, D., Dethloff, K., Ukita, J. and Yamazaki, K. (2016) Atmospheric autumn and winter response to Arctic sea ice changes in reanalysis data and model simulations. *Journal of Geophysical Research: Atmospheres*, 121, 7564–7577. https://doi.org/10.1002/2015JD024679.

Keenlyside, N. and Omrani, N.-E. (2014) Has a warm North Atlantic contributed to recent European cold winters? *Environmental Research Letters*, 9(6), 061001.

Kidston, J., Scaife, A.A., Hardiman, C., Mitchell, D.M., Butchart, N., Baldwin, M.P. and Gray, L.J. (2015) Stratospheric influence on tropospheric jet streams, storm tracks and surface weather. *Nature Geoscience*, 8, 433–440.

Kim, B.-M., Son, S.-W., Min, S.-K., Jeong, J.-H., Kim, S.-J., Zhang, X., Shim, T. and Yoon, J.-H. (2014) Weakening of the stratospheric polar vortex by Arctic Sea-ice loss. *Nature Communications*, 5, 4646.

Koenigk, T., Caian, M., Nikulin, G. and Schimanke, S. (2016) Regional Arctic Sea ice variations as predictor for winter climate conditions. *Climate Dynamics*, 46, 317–337. https://doi.org/10.1007/s00382-015-2586-1.

Kohonen, T. (2001) *Self-Organizing Maps*. Berlin: Springer, p. 501.

Kolstad, E.W., Bracegirdle, T.J. and Seierstad, I.A. (2009) Marine cold-air outbreaks in the North Atlantic: temporal distribution and associations with large-scale atmospheric circulation. *Climate Dynamics*, 33, 187–197.

Kornhuber, K., Petoukhov, V., Karoly, D., Petri, S., Rahmstorf, S. and Coumou, D. (2017) Summertime planetary wave resonance in the northern and southern hemispheres. *Journal of Climate*, 30, 6133–6150.

Kretschmer, M., Coumou, D., Donges, J.F. and Runge, J. (2016) Using causal effect networks to analyze different Arctic drivers of mid-latitude winter circulation. *Journal of Climate*, 29, 4069–4081. https://doi.org/10.1175/JCLI-D-15-0654.1.

Kug, J.-S., Jeong, J.-H., Jang, Y.-S., Kim, B.-M., Folland, C.K., Min, S.-K. and Son, S.-W. (2015) Two distinct influences of Arctic warming on cold winters over North America and East Asia. *Nature Geoscience*, 8, 759–762.

Lim, Y.-K. (2015) The East Atlantic/West Russia (EA/WR) tele-connection in the North Atlantic: climate impact and relation to Rossby wave propagation. *Climate Dynamics*, 44, 3211–3222.

Mann, M.E., Rahmstorf, S., Kornhuber, K., Steinman, B.A., Miller, S. K. and Coumou, D. (2017) Influence of anthropogenic climate change on planetary wave resonance and extreme weather events. *Scientific Reports*, 7, 45242. https://doi.org/10.1038/srep45242.

Marshall, J., Johnson, H. and Goodman, J. (2001a) A study of the inter-action of the North Atlantic oscillation with ocean circulation. *Journal of Climate*, 14, 1399–1421.

Marshall, J., Kushnir, Y., Battisti, D., Chang, P., Czaja, A., Dickson, R., Hurrell, J., McCartney, M., Saravanan, R. and Visbeck, M. (2001b) North Atlantic climate variability: phenomena, impacts and mechanisms. *International Journal of Climatology*, 21, 1863–1898.

Masato, G., Woollings, T. and Hoskins, B.J. (2014) Structure and impact of atmospheric blocking over the euro-Atlantic region in present-day and future simulations. *Geophysical Research Letters*, 41, 1051–1058. https://doi.org/10.1002/2013GL058570.

McCusker, K.E., Fyfe, J.C. and Sigmond, M. (2016) Twenty-five win-ters of unexpected Eurasian cooling unlikely due to Arctic Sea ice loss. *Nature Geoscience*, 9, 838–842.

McGraw, M. and Barnes, E.A. (2016) Seasonal sensitivity of the Eddy-driven jet to tropospheric heating in an idealized AGCM. *Journal of Climate*, 29, 5340.

Nakamura, T., Yamazaki, K., Iwamoto, K., Honda, M., Miyoshi, Y., Ogawa, Y. and Ukita, J. (2015) A negative phase shift of the winter AO/NAO due to the recent Arctic Sea-ice reduction in late autumn. *Journal of Geophysical Research – Atmospheres*, 120, 3209–3227.

Overland, J.E. and Wang, M. (2018) Resolving future Arctic/midlatitude weather connections. *Earth's Future*, 6(8), 1146–1152.

Overland, J., Francis, J., Hall, R., Hanna, E., Kim, S.-J. and Vihma, T. (2015) The melting Arctic and mid-latitude weather patterns: are they connected? *Journal of Climate*, 28, 7917–7932.

Overland, J.E., Dethloff, K., Francis, J.A., Hall, R.J., Hanna, E., Kim, S.-J., Screen, J.A., Shepherd, T.G. and Vihma, T. (2016) The melting Arctic and Midlatitude weather patterns: forced chaos and a way forward. *Nature Climate Change*, 6, 992–999.

Overland, J.E., Wang, M. and Box, J.E. (2019) An integrated index of recent pan-Arctic climate change. *Environmental Research Letters*, 14, 035006. https://doi.org/10.1088/1748-9326/aaf665.

Pedersen, R.A., Cvijanovic, I., Langen, P.L. and Vinther, B.M. (2016) The impact of regional Arctic Sea ice loss on atmospheric circulation and the NAO. *Journal of Climate*, 29, 889–902.

Peings, Y. and Magnusdottir, G. (2014) Forcing of the wintertime atmospheric circulation by the multidecadal fluctuations of the North Atlantic Ocean. *Environmental Research Letters*, 9(3), 034018.

Petoukhov, V., Rahmstorf, S., Petri, S. and Schellnhuber, H.J. (2013) Quasiresonant amplification of planetary waves and recent northern hemisphere weather extremes. *Publication National Academy of Sciences*, 110(14), 5336–5341.

Munich Re (2018), NatCatService, https://www.munichre.com/topics-online/en/climate-change-and-natural-disasters/climate-change/climate-change-heat-records-and-extreme-weather.html

Saha, S., Moorthi, S., Pan, H.-L., Wu, X., Wang, J., Nadiga, S., Tripp, P., Kistler, R., Woollen, J., Behringer, D., Liu, H., Stokes, D., Grumbine, R., Gayno, G., Wang, J., Hou, Y.T., Chuang, H.Y., Juang, H.M.H., Sela, J., Iredell, M., Treadon, R., Kleist, D., van Delst, P., Keyser, D., Derber, J., Ek, M., Meng, J., Wei, H., Yang, R., Lord, S., van den Dool, H., Kumar, A., Wang, W., Long, C., Chelliah, M., Xue, Y., Huang, B., Schemm, J.K., Ebisuzaki, W., Lin, R., Xie, P., Chen, M., Zhou, S., Higgins, W., Zou, C.Z., Liu, Q., Chen, Y., Han, Y., Cucurull, L., Reynolds, R.W., Rutledge, G. and Goldberg, M. (2010) The NCEP climate forecast system reanalysis. *Bulletin of the American Meteorological Society*, 91, 1015–1057.

Sato, K., Inoue, J. and Watanabe, M. (2014) Influence of the Gulf stream on the Barents Sea ice retreat and Eurasian coldness during early winter. *Environmental Research Letters*, 9, 084009.

Screen, J.A. (2014) Arctic amplification decreases temperature variance in northern mid- to high-latitudes. *Nature Climate Change*, 4, 577–582.

Screen, J.A. (2017) Simulated atmospheric response to regional and pan-Arctic Sea ice loss. *Journal of Climate*, 30, 3945–3962.

Screen, J.A., Deser, C., Simmonds, I. and Tomas, R. (2014) Atmospheric impacts of Arctic Sea-ice loss, 1979-2009: separating forced change from atmospheric internal variability. *Climate Dynamics*, 43, 333–344.

Serreze, M.C., Barrett, A.P. and Cassano, J.J. (2011) Circulation and surface controls on the lower tropospheric temperature field of the Arctic. *Journal of Geophysical Research*, 116, D07104.

Singarayer, J., Bamber, J. and Valdes, P. (2006) Twenty-first-century climate impacts from a declining Arctic Sea ice cover. *Journal of Climate*, 19, 1109–1125.

Smith, K.L., Fletcher, C.G. and Kushner, P.J. (2010) The role of linear interference in the annular mode response to extra-tropical surface forcing. *Journal of Climate*, 23, 6036–6050.

Smith, D., Dunstone, N.J., Scaife, A.A., Fiedler, E.K., Copsey, D. and Hardiman, S.C. (2017) Atmospheric response to Arctic and Antarctic Sea ice: the importance of ocean-atmosphere coupling and the background state. *Journal of Climate*, 30, 4547–4565.

Straus, D.M., Corti, S. and Molteni, F. (2007) Circulation regimes: chaotic variability versus SST-forced predictability. *Journal of Climate*, 20, 2251–2272.

Trenberth, K.E. (1991) Climate diagnostics from global analysis: conservation of mass in ECMWF analysis. *Journal of Climate*, 4, 707–721.

Trenberth, K.E. and Fasullo, J.T. (2013) An apparent hiatus in global warming? *Earth's Future*, 1, 19–32.

Vautard, R. (1990) Multiple weather regimes over the North Atlantic: analysis of precursors and successors. *Monthly Weather Review*, 118(10), 2056–2081.

Vavrus, S.J. (2018) The influence of Arctic amplification on mid-latitude weather and climate. *Current Climate Change Reports.*, 4, 238–249.

Vavrus, S.J., Wang, F., Martin, J., Francis, J., Peings, Y. and Cattiaux, J. (2017) Changes in north American atmospheric circulation and

extreme weather: influence of Arctic amplification and northern hemisphere snow cover. *Journal of Climate*, 30, 4317–4333.

Vihma, T. (2014) Effects of Arctic Sea ice decline on weather and climate: a review. *Surveys in Geophysics*, 35, 1175–1214.

Vihma, T. (2017) Weather extremes linked to interaction of the Arctic and mid-latitudes. In: Wang, S.-Y., et al. (Eds.) *Climate Extremes: Mechanisms and Potential Prediction*. Hoboken, NJ: John Wiley & Sons, Inc., pp. 39–49.

Vihma, T., Cheng, B., Uotila, P., Wei, L. and Qin, T. (2014) Linkages between Arctic Sea ice cover, large-scale atmospheric circulation, and weather and ice conditions in the Gulf of Bothnia, Baltic Sea. *Advances in Polar Science*, 4, 289–229.

Wu, Y. and Smith, K.L. (2016) Response of northern hemisphere mid-latitude circulation to Arctic amplification in a simple atmospheric general circulation model. *Journal of Climate*, 29, 2041–2058.

Yang, S. and Christensen, J.H. (2012) Arctic Sea ice reduction and European cold winters in CMIP5 climate change experiments. *Geophysical Research Letters*, 39, L20707.

Yeager, S.G. and Robson, J.I. (2017) Recent progress in understanding and predicting Atlantic decadal climate variability. *Current Climate Change Reports*, 3(2), 112–127.

Yiou, P. and Nogaj, M. (2004) Extreme climatic events and weather regimes over the North Atlantic: when and where? *Geophysical Research Letters*, 31, L07202.

Yue, S. and Wang, C. (2004) The Mann-Kendall test modified by effective sample size to detect trend in serially correlated hydrological series. *Water Resources Management*, 18(3), 201–218.

Zappa, G. and Shepherd, T.G. (2017) Storylines of atmospheric circulation change for European regional climate impact assessment. *Journal of Climate*, 30, 6561–6577.

Zappa, G., Pithan, F. and Shepherd, T.G. (2018) Multimodel evidence for an atmospheric circulation response to Arctic Sea ice loss in the CMIP5 future projections. *Geophysical Research Letters*, 45, 1011–1019.

Zeng, J., Matsunaga, T. and Mukai, H. (2010) METEX – a flexible tool for air trajectory calculation. *Environmental Modelling & Software*, 25, 607–608.

Zhang, P., Wu, Y., Simpson, I.R., Smith, K.L., Zhang, X., De, B. and Callaghan, P. (2019) A stratospheric pathway linking a colder Siberia to Barents-Kara Sea Sea ice loss. *Science Advances*, 4, eaat6025.

SUPPORTING INFORMATION

Additional supporting information may be found online in the Supporting Information section at the end of this article.